AN ABSTRACT OF THE THESIS OF

Laure Honorez for the degree of Master of Science in Chemical Engineering presented on January 25, 1994.

Title: Fluid Dynamic Characteristics of a Magnetically Stabilized Liquid-Solid Fluidized Bed.

Redacted for Privacy

Abstract approved: _____
Goran Jovanovic

Most of the experimental results in the studies of magnetically stabilized fluidized beds, MSFBs, found in literature did not take into account magnetic properties of the magnetic particles. As a consequence, reported data correlations can be applied only for particular experimental conditions. No general design equation, which would be valid for different types of materials, fluid velocities and magnetic field intensities was ever presented.

In this study, we investigate the behaviour of magnetically stabilized liquid-solid fluidized beds in an axial uniform and time-invariant magnetic field. The magnetic field is generated by a copper coil wound around the fluidization column. Fields from zero to 16 000 A/m are produced. We use two types of particles, A and B ($125 \leq d_p \leq 833$ μm for particles A; $1397 \leq d_p \leq 2380$ μm for particles B). Particles are ferromagnetic ($\chi = 9.377\ 10^{-5}\ H + 1.288$ for particles A; $\chi = 1.814\ 10^{-4}\ H + 6.28$ for particles B). Water at room temperature is the fluidizing fluid.

Maps of fluidization regimes for both types of particles show four different operating regimes: the packed bed, stabilized, partially stabilized and random

motion regimes. The pressure drop through the bed is measured at fourteen locations along the fluidization column. The pressure drop data are used to evaluate the average bed porosity of the bed. An equation was found to predict the average bed porosity for given particles, fluid velocity and magnetic field intensity: $\varepsilon = \varepsilon_{ms} + (\varepsilon_{ff} - \varepsilon_{ms}) \exp(-(1-\varepsilon)(M / H_{ms}))$ where $M = \chi H = (\alpha H + \beta) H$.

Magnetic properties of the particles, namely the magnetization intensity M, play a major role in the behaviour of MSFBs. Introduction of magnetization intensity in the above equation is the key to the modeling of average bed porosity. It allows the model to be applicable to different types of ferromagnetic particles, which is an improvement to previous correlations.

Fluid Dynamic Characteristics of a Magnetically Stabilized Liquid-Solid Fluidized Bed

by

Laure Honorez

A THESIS

submitted to

Oregon State University

in partial fulfillment of
the requirement for the
degree of

Master of Science

Completed January 25, 1994

Commencement June 1994

APPROVED:

Redacted for Privacy

Professor of Chemical Engineering in charge of major

Redacted for Privacy

Head of Department of Chemical Engineering

Redacted for Privacy

Dean of the Graduate School

Date thesis is presented January 25, 1994.

Typed by Laure Honorez for Laure Honorez.

TABLE OF CONTENTS

LIST OF FIGURES

LIST OF TABLES

NOTATION

a	Constant parameter in (Eq. 5-4)	(m/A)
a_1	Parameter in (Eq. D-2)	(undefined)
a_2	Parameter in (Eq. D-2)	(undefined)
a_3	Parameter in (Eq. D-9)	(undefined)
A	Column cross section	(m^2)
b	Fitting parameter in (Eq. 6-1 and 6-2)	(/)
c	Fitting parameter in (Eq. 6-1 and 6-2)	(m/A)
C_D	Drag coefficient in (Eq. 2-4 and 2-5) (Kunii and Levenspiel, 1991)	(/)
d_p	Particle diameter	(m)
D	Column diameter	(m)
F_b	Buoyancy force exerted on a particle	(N)
F_d	Drag force exerted on a particle	(N)
F_g	Gravitational force exerted on a particle	(N)
g	Gravitational acceleration	(m/s^2)
g_c	Conversion factor (in Eq. 5-2)	(kg m/N s^2)
H	Magnetic field intensity	(A/m)
H_{ms}	Magnetic field intensity at the transition between the partially stabilized and the stabilized regimes	(A/m)
H_{mr}	Magnetic field intensity at the transition between the random motion and the partially stabilized regimes	(A/m)
H_0	Characteristic magnetic field strength (Kwauk et al., 1992) (Eq. 5-3)	(A/m)
i	Index	(/)
I	Electric current intensity	(A)
j	Index (in Appendix D)	(/)

J	Number of experimental data points (in Appendix D)	(/)
k	Fitting parameter in (Eq. 6-10)	(/)
L	Bed height	(cm)
L_i	Height of the i^{th} pressure port above the distributor	(m)
m	Length of the solenoid	(m)
M	Magnetization intensity	(A/m)
M_{mc}	Magnetization intensity at the transition between the partially stabilized and the stabilized regimes	(A/m)
n	Richardson-Zaki coefficient in (Eq. 2-2 and 2-3) (Leva, 1959)	(/)
N	Number of turns in the solenoid	(/)
P_i	Pressure in the i^{th} probe	(Pa)
R	Electric circuit resistance	(Ω)
R^2	Regression coefficient	(/)
Re_p	Particle Reynolds number $\left(= \frac{d_p \rho U_0}{\mu} \right)$	(/)
s	Parameter (in Eq. 5-3)	(/)
SS	Sum of squares (in Appendix D)	(/)
U	Voltage applied to the solenoid (in Appendix C)	(V)
U_{ms}	Water superficial velocity at the transition from the partially stabilized to the stabilized regimes	(m/s)
U_{mr}	Water superficial velocity at the transition from the random motion to the partially stabilized regimes	(m/s)
U_{mf}	Minimum fluidization velocity	(m/s)
U_t	Terminal velocity	(m/s)
U_0	Water superficial velocity	(m/s)
U_{0max}	Maximum water superficial velocity	(m/s)
V_ε	Void function (in Eq. 5-4) (Jovanovic et al., 1993)	(/)
W	Weight of particles in the bed	(kg)

W_f	Weight of fluidized particles in the bed (in Eq. 6-6)	(kg)
x	Explanatory variable (in Appendix D)	(undefined)
y	Predicted value (in Appendix D)	(undefined)
Y	Experimental value (in Appendix D)	(undefined)

Greek symbols

α	Linear coefficient in the expression of χ as a function of H in (Eq. 2-6)	(m/A)
β	Constant coefficient in the expression of χ as a function of H in (Eq. 2-6)	(/)
ΔP_{bed}	Pressure drop across the bed	(Pa)
ΔP_f	Pressure drop due to frictional forces between particles and vessel walls in (Eq. 6-6)	(Pa)
ΔP_i	Pressure drop across the portion of the bed between the distributor and the i^{th} pressure port level	(Pa)
ΔP_m	Pressure drop due to the net attractive magnetic force in (Eq. 6-6)	(Pa)
ε	Average bed porosity	(/)
ε_{ff}	Average bed porosity for H=0	(/)
ε_M	Average bed porosity in the stabilized regime in (Eq. 5-3) (Kwauk et al., 1992)	(/)
ε_{ms}	Average bed porosity at the transition between the partially stabilized and the stabilized regimes	(/)
ε_{mf}	Bed porosity at onset of fluidization	(/)
ε_P	Bed porosity in the random motion regime in (Eq. 5-3) (Kwauk et al., 1992)	(/) (/)
Φ_s	Particle shape factor	(/)
μ	Fluid viscosity	(kg/m s)
ρ	Fluid density	(kg/m^3)

ρ_p	Particle density	(kg/m^3)
χ	Particle magnetic susceptibility	(/)

Subscripts

ff	Free fluidization
i	Pressure port number (from 0 to 14)
M	Magnetically condensed regime
ms	Transition between partially stabilized and stabilized regimes
mf	Minimum fluidization
mr	Transition between random motion and partially stabilized regimes
p	Particle

FLUID DYNAMIC CHARACTERISTICS OF A MAGNETICALLY STABILIZED LIQUID - SOLID FLUIDIZED BED

CHAPTER 1
INTRODUCTION

Magnetically stabilized fluidized beds, MSFBs, are a special class of fluidized beds; an external magnetic field is used to control the dynamic behaviour of fluid and solids in the bed. The presence of the magnetic field alters the motion of ferromagnetic particles in MSFBs, thus creating conditions for other changes in fluidized beds characteristics. The most important change is the change in the beds structure: particles align themselves along the field lines, forming chains of different lengths. Using this and other effects of magnetic field, one can change the contacting patterns between fluid and solids. Fluid can flow with a higher flow rate in MSFBs than in conventional beds, without elutriating particles from the bed or breaking catalyst. The features of MSFBs may be used to control heat and mass transfer rate in MSFBs, thus improving performance and overcoming some shortcomings of conventional beds.

The earliest study in this area was done by Filippov in 1960. He even proposed an application for this new type of fluidized beds: "The *pseudopolymerized* regime could be used as a host medium to separate solids." Since then, MSFBs have found many applications. Among them:

1 - bubble suppression in gas fluidization (Rosensweig, 1979),

2 - filtration of solids through a layer of ferromagnetic particles (Kwauk et al., 1992),

3 - magnetic valve design for control of particle flow (Moiset and Dartois, 1960; Kwauk, 1977; Wang et al., 1982),

4 - magnetic distributor design for control of residence time distribution (Jaraiz et al., 1984; Davis and Levenspiel, 1985),

5 - magnetic elevator for particles (Wallace et al., 1991).

Liquid-solid MSFBs find a particular application in the development of new wastewater treatment processes, chromatography techniques, high-rate chemical and biochemical processes (Terranova and Burns, 1991; Burns and Graves, 1985; Sada et al., 1985).

While extensive studies were conducted in gas-solid MSFBs, attention was less focused on liquid-solid MSFBs. It is well known from previous studies, that when a magnetic field is applied to a liquid-solid MSFB, the bed height and the porosity decrease whereas the pressure drop across the bed is found to be constant. However, no general equation is readily available to predict the average bed voidage for given particles, magnetic field intensity and fluid superficial velocity. In this work, the structure of liquid-solid MSFBs is studied. Experimental data related to the bed voidage and magnetic properties of the particles are used to find an equation predicting the bed porosity for given operating conditions.

Chapters 2 to 4 deal with instrumentation , experimental procedures, and data conversion. Chapter 5 is a review of fundamental background in MSFBs. Chapter 6 presents our experimental results and gives an interpretation of them.

CHAPTER 2
APPARATUS

A schematic representation of the experimental equipment is shown in Figure 2-1. The apparatus consists of several parts:

1 - the fluidization column with particles,

2 - the water supply system,

3 - the pressure measuring system,

4 - the magnetic field generator.

2.1 - The fluidization column with particles

The fluidization column: The column in which the particles are fluidized is made of Plexiglas, allowing visual observation through the walls. It is assembled from two removable parts:

1 - the bottom part is a 380 mm long tube, 90 mm internal diameter. The distributor plate sits at 300 mm from the bottom and can be replaced,

2 - the upper part is a 1 m long pipe, 75 mm internal diameter, which fits into the bottom part and sits on the distributor plate.

The distributor plate is a perforated Plexiglas plate, 3 mm thick and 73 mm in diameter. It has one hundred 1/16 inch circular holes. The plate is covered with plastic wire-mesh screen which prevents particles from falling below the distributor when the bed is not fluidized. The pressure drop across the distributor as a function of water velocity is shown in appendix A.

Figure 2-1: Schematic representation of the experimental equipment

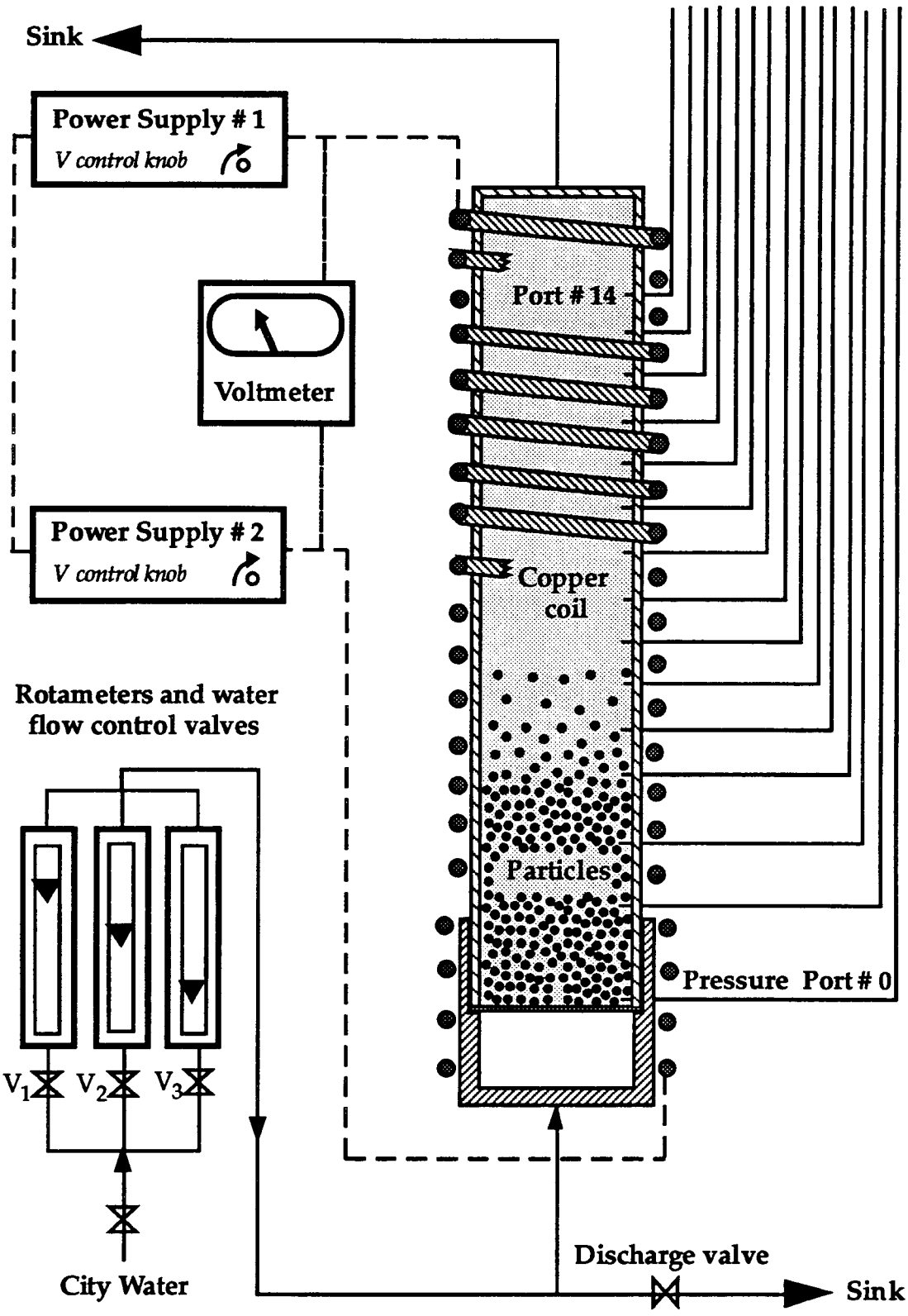

Fifteen pressure ports on the column wall are used for pressure measurements. Their locations are reported in Table 2-2.

The bed is operated at room temperature and atmospheric pressure.

The particles: Two types of magnetizable particles are used. Their properties are summarized in Table 2-1.

The particles are sieved and their densities are determined from volumetric and weight measurements in water.

Minimum fluidization velocities for both types of particles are evaluated from pressure drop measurements on $\log(\Delta P_{bed})$ versus superficial velocity diagram. Figures 2-2 and 2-3 show this diagram for the A and the B type particles. Obtained values match visual observations and values extimated from the correlation by Chitester et al. (1984) for coarse particles:

$$\frac{d_p U_{mf} \rho}{\mu} = \left[28.7^2 + 0.0494 \left(\frac{d_p \rho (\rho_p - \rho) g}{\mu^2} \right) \right]^{0.5} - 28.7 \qquad \text{(Eq. 2-1)}$$

The error between the experimental and the estimated values is less than 7%.

Terminal velocities for both types of particles are evaluated from the Richardson-Zaki equation when the bed is fluidized in absence of magnetic field (Leva, 1959):

$$\frac{U_0}{U_t} = \varepsilon^n \qquad \text{(Eq. 2-2)}$$

$$n = \left(4.45 + 18 \frac{d_p}{D}\right) Re_p^{-0.1} \qquad \text{(Eq. 2-3)}$$

Table 2-1: Particles properties

Particles Type	d_p range (μm)	Mean d_p (μm)	ρ_p (kg/m^3)	Φ_s (/)	$\chi = \alpha H + \beta$		U_{mf} exp* (cm/s)	U_{mf} (Eq. 2-1) (cm/s)	ε_{mf} exp* (/)	U_t exp* (cm/s)	U_t (Eq. 2-4) (cm/s)
					α (m/A)	β (/)					
A	125 - 833	480	2700	0.80	$9.377\ 10^{-5}$	1.288	0.30	0.32	0.45	6.25	6.77
B	1397 - 2380	1880	2450	0.75	$1.814\ 10^{-4}$	6.28	2.30	2.42	0.42	18.32	17.00

* exp = experimental values

Figure 2-2: Experimental measurement of the minimum fluidization velocity for particles A

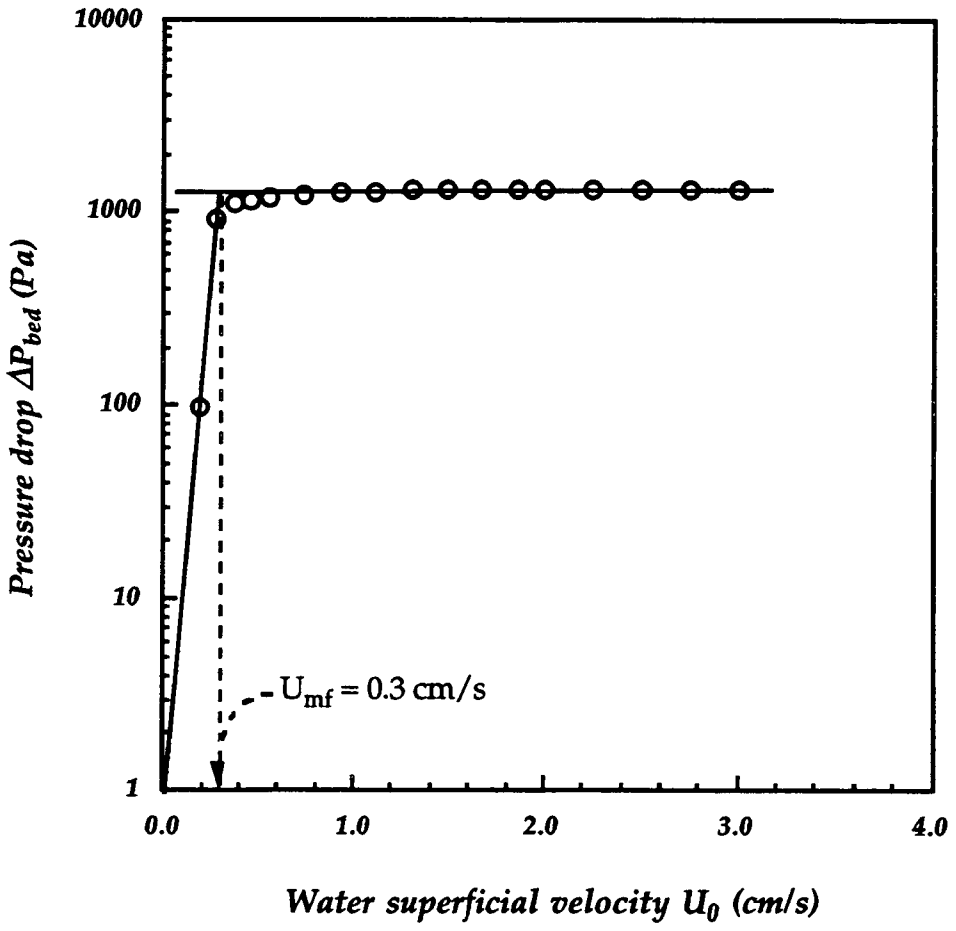

Figure 2-3: Experimental measurement of the minimum fluidization velocity for particles B

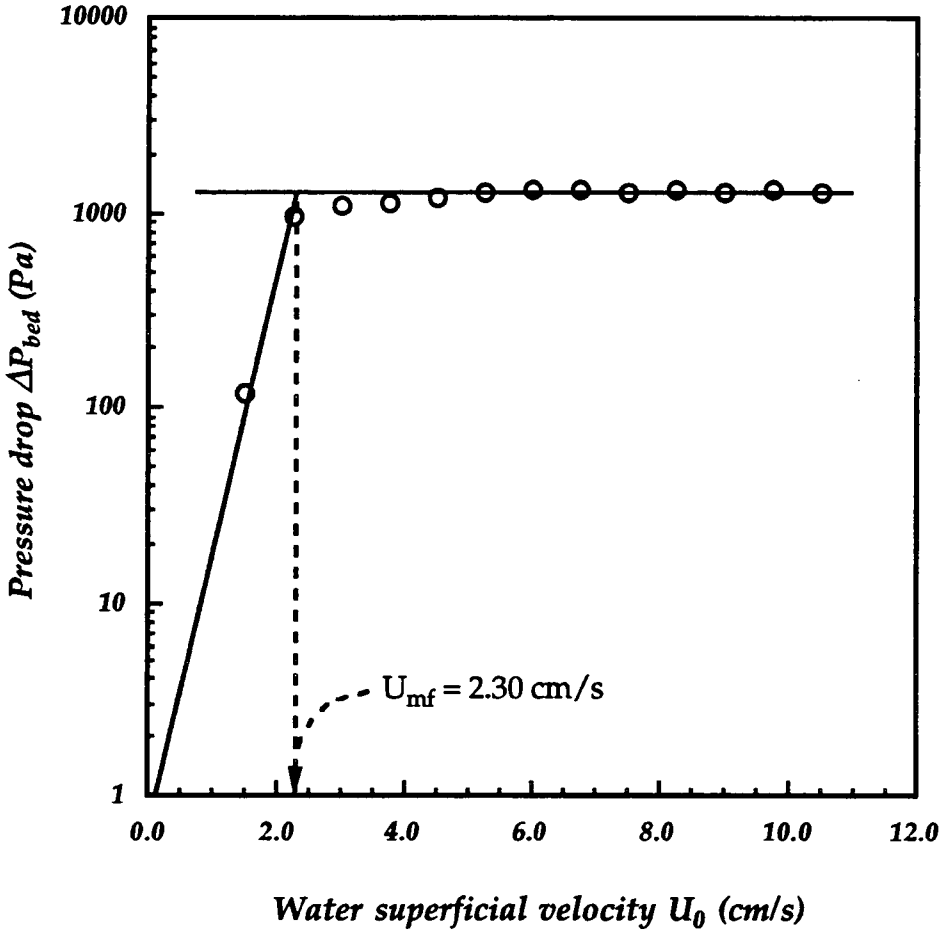

The slope of the line on U_0 versus ε^n plot represents the terminal velocity of the particles, U_t. This is shown in Figure 2-4 for the A and the B type particles. Experimentally obtained values match estimated values from the equation given by Kunii and Levenspiel (1991):

$$U_t = \left[\frac{4\, d_p\, (\rho_p - \rho)}{3\, \rho\, C_D} \right]^{0.5} \qquad \text{(Eq. 2-4)}$$

$$C_D = \frac{24}{Re_p} \left(1 + 8.1716 \exp(-4.0655\, \Phi_s)\, Re_p^{(0.0964 + 0.5565\, \Phi s)} \right) + \frac{73.69 \exp(-5.0748\, \Phi_s)\, Re_p}{Re_p + 5.378 \exp(6.2122\, \Phi s)} \qquad \text{(Eq. 2-5)}$$

The error between the experimental and the calculated values of U_t is less than 8%.

Values of the porosity at the minimum fluidization conditions are determined experimentally as explained later in Chapter 6. They are in good agreement with the data available in the literature (Kunii and Levenspiel, 1991).

An important particle characteristic, especially for this study, is magnetic susceptibility. Typically magnetic susceptibility of ferromagnetic material is found to be a linear function of the magnetic field strength (Arnaldos et al., 1985; Reitz et al., 1992):

$$\chi = \alpha H + \beta \qquad \text{(Eq. 2-6)}$$

A basic equation in magnetostatics gives a relationship between magnetization intensity M and magnetic field strength H (Reitz et al., 1992):

$$M = \chi\, H = \alpha H^2 + \beta H \qquad \text{(Eq. 2-7)}$$

Figure 2-4: Terminal velocity determination for particles A and B

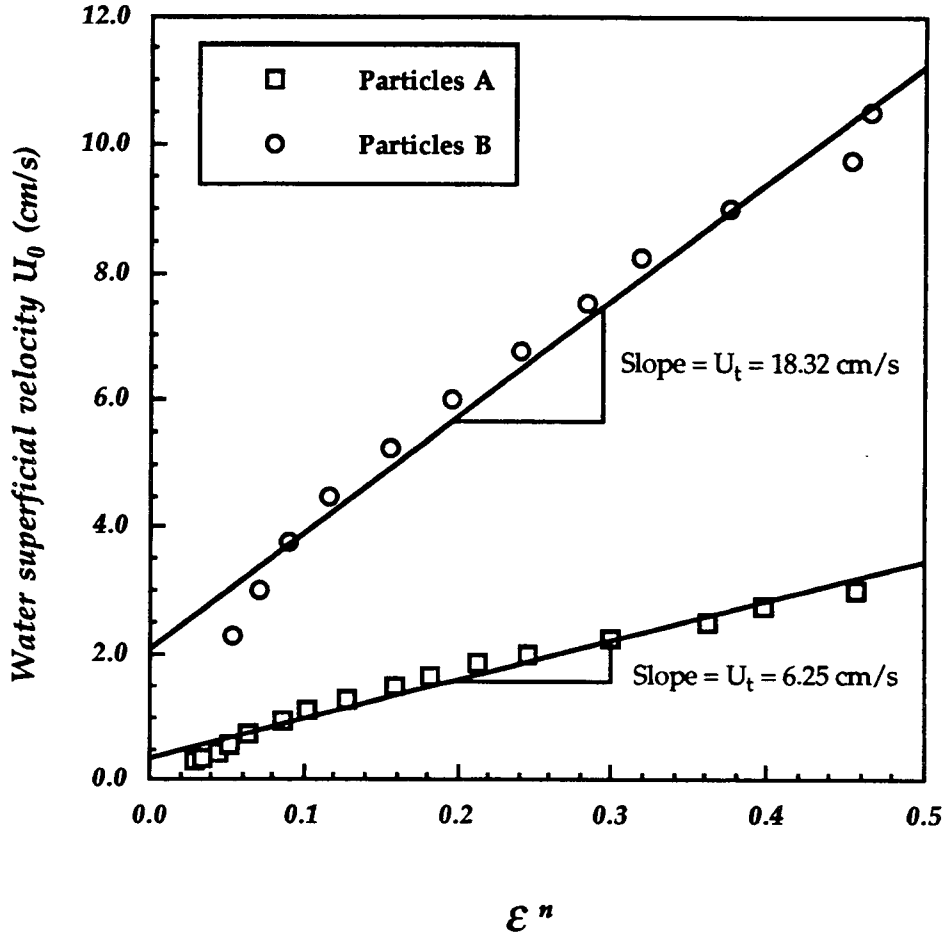

From this equation, we can derive:

$$\frac{dM}{dH} = 2\alpha H + \beta \qquad \text{(Eq. 2-8)}$$

The coefficient β in Equation 2-6 can be easily found from standard magnetization curves, which display M versus H. It is the slope of the curve at the origin:

$$\beta = \left[\frac{dM}{dH}\right]_{H=0} \qquad \text{(Eq. 2-9)}$$

The magnetization curves of the particles A and B are shown in Appendix B. Magnetic susceptibilities are also plotted against the magnetic field intensity in Appendix B for both types of particles. Typically, the relationship between M and H shows an hysteresis phenomenon. However, for our materials, the magnetization curves are obtained for low magnetic field intensities (from 0 to 3.5 kA/m) and present a very small hysteresis. Therefore, they do not allow us to accurately determine α, which is, in all probabilities, a very small number. α is found later by adjusting the experimental parameters for Equation 6-7.

In our experiments, we never reached the magnetic saturation of the particles before getting to the stabilized regime.

2.2 - The water supply system

Water from the city supply network is used. The water flow rate is measured by three different rotameters. Any desired flow rate of water from 0 to 0.5 l/s can be adjusted by appropriate combination of rotameters. Each rotameter was

previously calibrated with city water. Three valves (V_1, V_2 and V_3 in Figure 2-1) control the water flow rate at the inlet of each rotameter.

2.3 - The pressure measuring system

The pressure measuring system consists of a bank of fifteen piezometric glass tubes, 6 mm in diameter. Each of them is connected to its corresponding pressure port with 1/4 inch plastic tubing and a brass connector mounted on the column wall. Each pressure port is covered with plastic wire-mesh screen to prevent particles from entering the tubes.

The pressure ports location along the fluidization column are reported in Table 2-2.

2.4- The magnetic field generator

The magnetic field is created by passing direct electric current through a copper coil wound around the fluidization column. The copper tube is 1/4 inch tube wound in one hundred turns over one meter length. The copper coil and two power supplies are connected in series as shown in Figure 2-1. Each power supply can maintain a voltage drop across the solenoid between 0 and 5 V. The voltage is controlled at each power supply and monitored by a voltmeter of an appropriate range (in this case from 0 to 15 V) connected in parallel with the

Table 2-2: Location of the pressure ports along the column

Pressure port number	0	1	2	3	4	5	6	7
Height from the distributor (mm)	6	96	136	187	238	289	340	391

Pressure port number	8	9	10	11	12	13	14
Height from the distributor (mm)	442	493	543	594	646	697	766

copper coil. The total resistance of the electrical circuit (power supplies, solenoid, voltmeter, connecting wires) is 0.0504 Ω. Theoretically this arrangement allows to deliver electric current from 0 to 200 A, which can generate a magnetic field intensity from 0 to 20 000 A/m according to the following relationship:

$$H = \frac{I N}{m} \qquad \textbf{(Eq. 2-10)}$$

As current is applied to the solenoid, the solenoid has to be permanently cooled down. Water flowing inside the copper tube keeps the coil to a reasonable

temperature so that the resistance of the system can be considered constant. The practical range for the magnetic field intensity is from 0 to 16 000 A/m.

The accuracy of the voltage measurement is 0.05 V which is equivalent to a magnetic field of 100 A/m. The voltage-current calibration curve of the system is shown in Appendix C.

CHAPTER 3
EXPERIMENTAL PROCEDURES

The pressure drop across any section of the fluidized bed is a measure of the drag force exerted by the flowing fluid on solid particles. The pressure drop data are used to calculate the bed porosity ε which will be shown later (Chapter 4).

The pressure drop data were obtained in two different magnetization modes:

1 - the magnetization first mode,

2 - the fluidization first mode.

3.1 - The magnetization first mode

The procedure used to collect experimental pressure drop measurements in the magnetization first mode is described in Figure 3-1. The major feature of this mode of operation is that the magnetic field intensity is first set to a fixed value, and then the water velocity through the bed is increased and set to a desired value.

3.2 - The fluidization first mode

The procedure used to collect experimental pressure drop measurements in the fluidization first mode is described in Figure 3.2. The major feature of this mode

Figure 3-1: Pressure drop measurements procedure in "magnetization first" mode

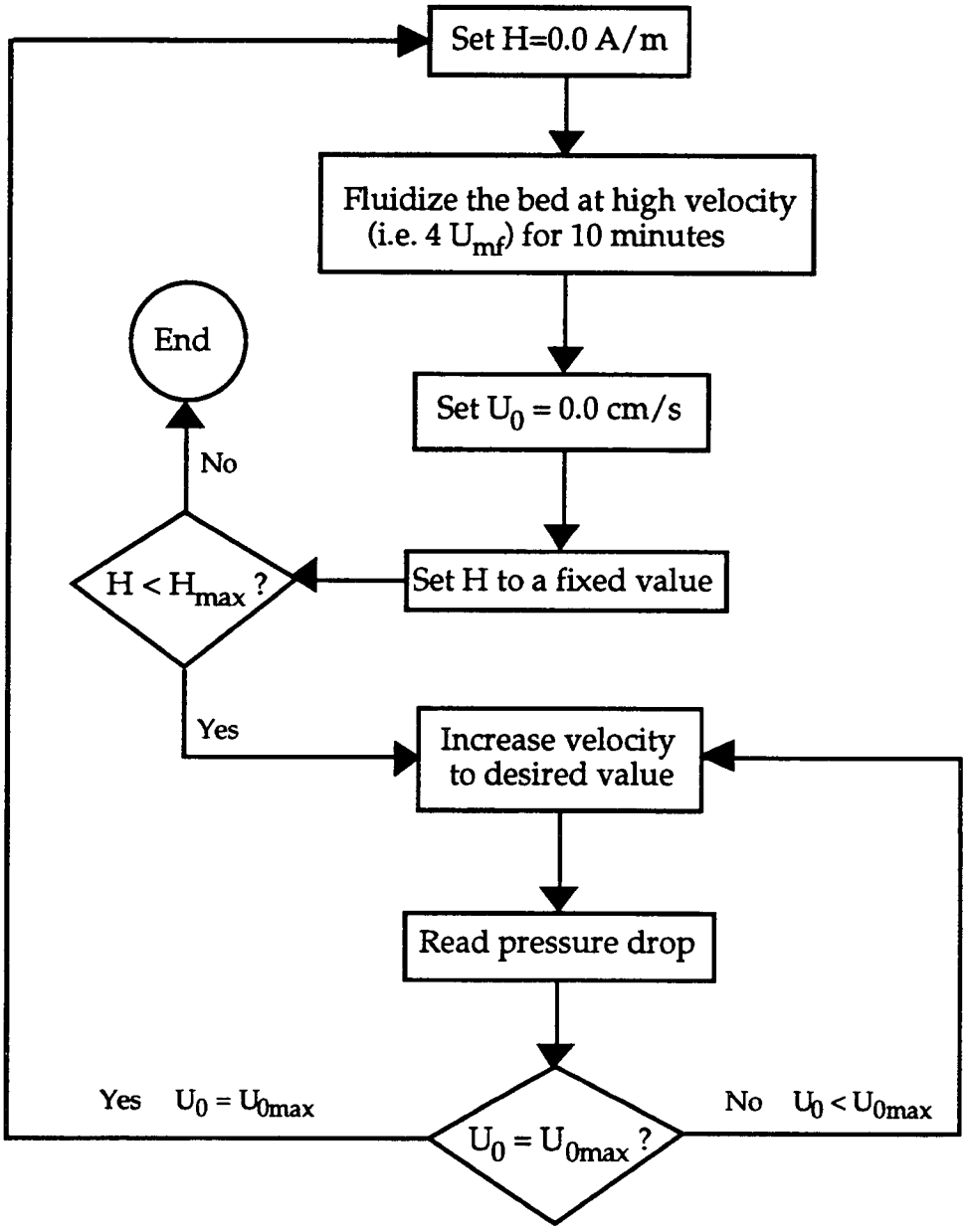

Figure 3-2: Pressure drop measurements procedure in "fluidization first" mode

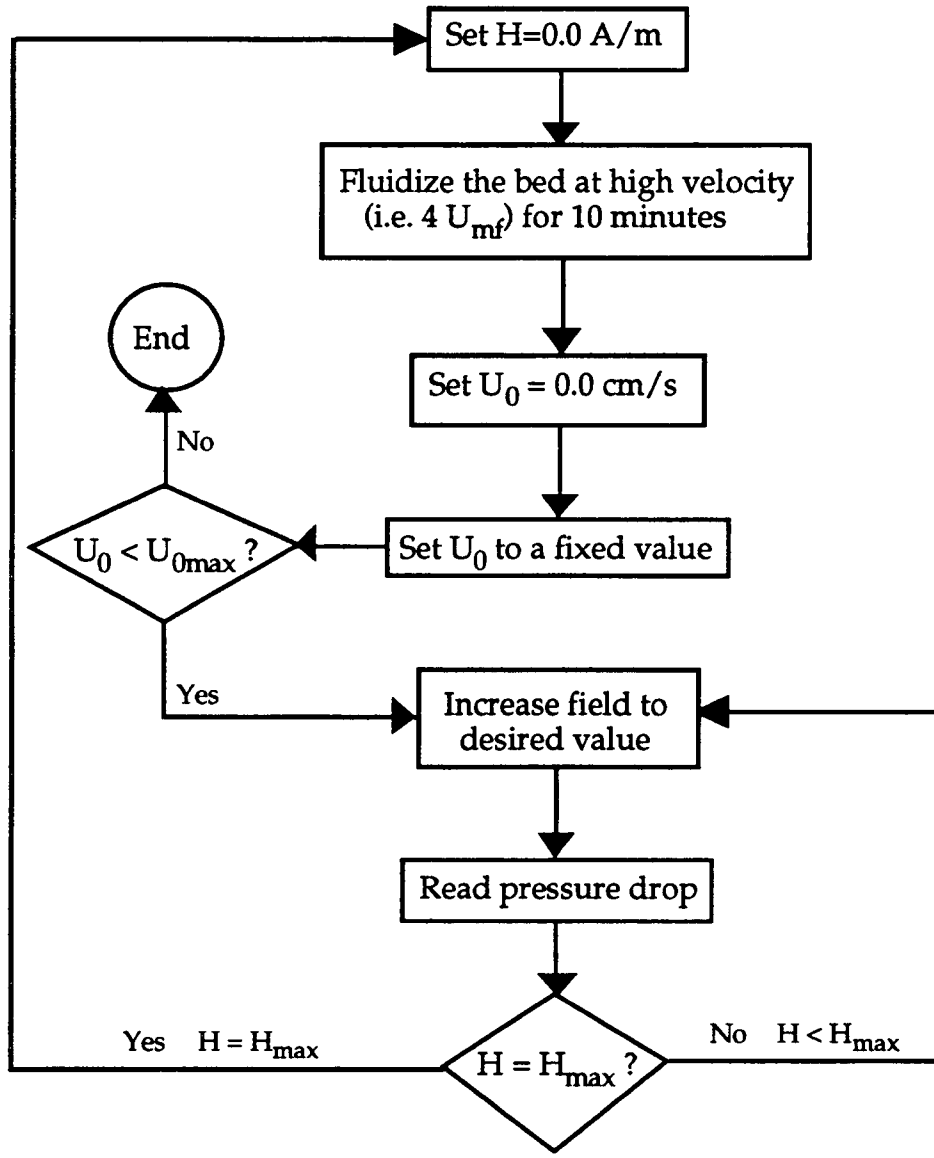

of operation is that the water flow rate is first set to a fixed value, and then the magnetic field strength is increased and set to a desired value.

3.3 - Common features to the two modes

Between any two successive measurements for two different magnetic field intensities in the magnetization first mode and in the fluidization first mode, the bed is fluidized for ten minutes to erase any remanence. This assures that all the measurements are done from the same initial conditions.

Table 3-1 Experimental parameters and conditions

Particles Type	U_0 range (cm/s)	$\frac{U_{0max}}{U_{mf}}$	W (kg)	H range (A/m)
A	0 - 3.00	10.0	0.560	0 - 15 900
B	0 - 10.50	4.57	0.592	0 - 15 900

Using these procedures we collected pressure drop data at each pressure probe for a variety of water velocities and magnetic field intensities in each of the two magnetization modes. Table 3-1 shows the range of experimental conditions.

The accuracy of the pressure drop calculation is estimated to be 2 mm of water column or 20 Pa. However the error involved is estimated to be 5 mm of water column or 50 Pa. This error is due to fluctuations of the pressure drop and a certain inertia in the response of the measuring system to these fluctuations.

CHAPTER 4
DATA CONVERSION

The pressure measurements at each of the fifteen locations along the column for given magnetization mode, water flow rate and magnetic field intensity are used to obtain data for:

1 - the overall pressure drop across the bed

2 - the bed height needed for porosity calculations

4.1 - The overall pressure drop across the bed

As long as the bed height is below the level of the fifteenth pressure port (port # 14 in Figure 2-1), the overall pressure drop across the bed can be calculated as:

$$\Delta P_{bed} = P_0 - P_{14} \qquad \textbf{(Eq. 4-1)}$$

Hence, we can calculate the overall pressure drop across the bed for any magnetization mode, velocity and magnetic field intensity at which data were recorded.

4.2 - The height of the bed

We can easily compute the pressure drop between the distributor plate and any pressure port:

$$\Delta P_i = P_i - P_0 \qquad \text{(Eq. 4-2)}$$

By plotting ΔP_i against L_i, where L_i is the height of the i^{th} pressure port, we can determine the bed height.

It is well known that in the fluidized bed, the porosity is not uniform along its height (Kunii and Levenspiel, 1991). The bed is more dense at the bottom and becomes leaner toward the top. We can visualize three different zones in the bed as shown in Figure 4-1. In each of the zones, we assume a constant porosity. Then the top of the bed is considered to have the same density as the upper zone. We can use the ΔP_i versus L_i curves to determine the bed height at given operating conditions. This procedure is shown in Figures 4-2 and 4-3: the bed height is found at the intersection of the lines (1) and (2).

By determining the bed height for given magnetization mode, water flow rate, and magnetic field intensity, we can calculate the average bed porosity:

$$\Delta P_{bed} = \frac{W}{A} = L\, g\, (\rho_p - \rho)\, (1 - \varepsilon) \qquad \text{(Eq. 4-3)}$$

$$\varepsilon = 1 - \frac{\Delta P_{bed}}{L\, g\, (\rho_p - \rho)} \qquad \text{(Eq. 4-4)}$$

At low fluidization velocities, the bed appears to have a uniform porosity which can be seen from the experimental data plotted in Figure 4-2. For higher fluidization velocities, distinct zones of different porosity can easily be detected (Figure 4-3).

Figure 4-1: Zones of constant porosity in a fluidized bed

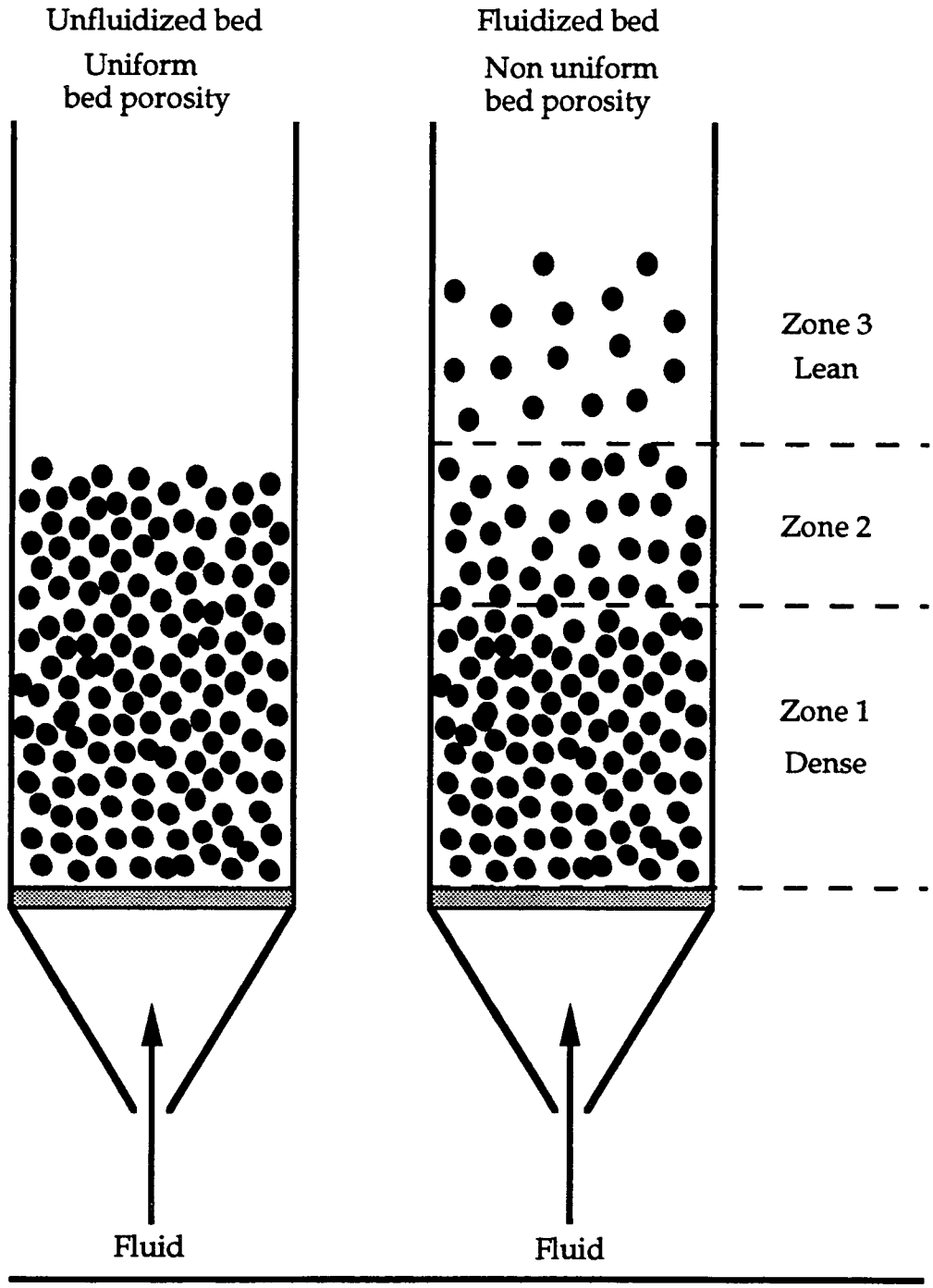

Figure 4-2: Bed height determination for a uniform bed porosity

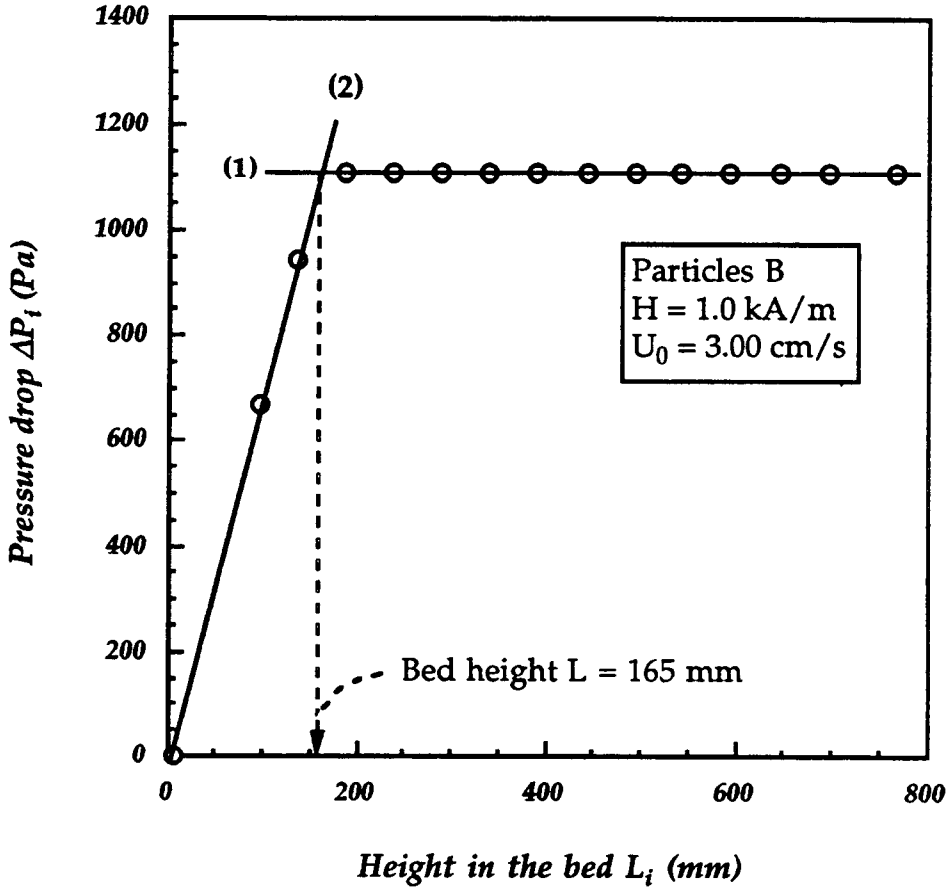

Figure 4-3: Bed height determination for a non uniform bed porosity

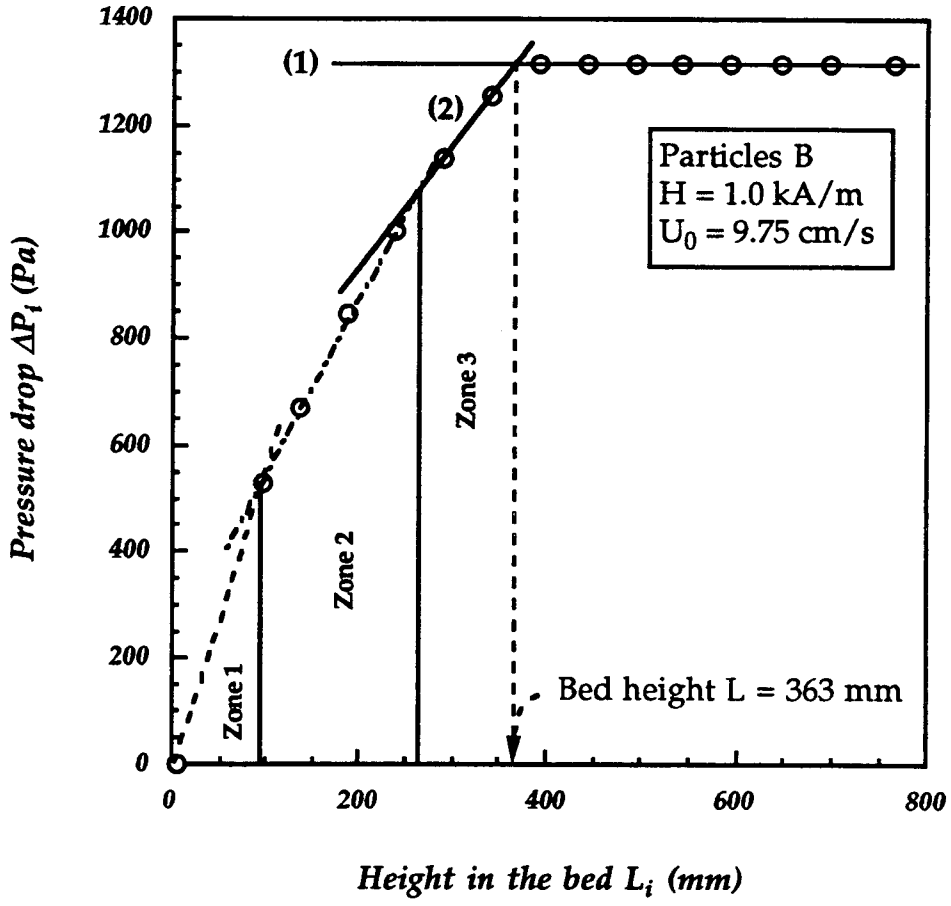

CHAPTER 5
FUNDAMENTAL BACKGROUND IN MSFBs

5.1 - Map of fluidization regimes in MSFBs

Several regimes of fluidization exist in magnetically stabilized fluidized beds. Siegell (1989) and Liu and coworkers (1991) presented a review of the fundamental and practical developments of MSFB.

First evidence of the different fluidization regimes in MSFB was reported by Kirko and Filippov (1960) and Filippov (1960, 1961, 1962). They studied the fluidization of iron particles in a liquid-solid bed. Their observations are displayed as a regime map or phase diagram in Figure 5-1. They identified the following regimes: the packed bed regime, the pseudopolymerized regime, a regime showing some particle motion, a regime showing extensive particle mixing and a regime where particles are entrained from the bed. Equivalent terminology for these regimes was used by different authors. Table 5-1 summarizes some of the terms used in liquid-solid MSFBs.

Figure 5-2 shows a typical regime map for MSFBs. Following arrow A in Figure 5-2 for a fixed low magnetic field intensity and increasing fluid velocity, five different regimes are encountered:

1 - packed bed (between points A1 and A2): it appears that the magnetic field has no influence on this regime,

Figure 5-1: Phase diagram from Filippov (Liu, 1992)

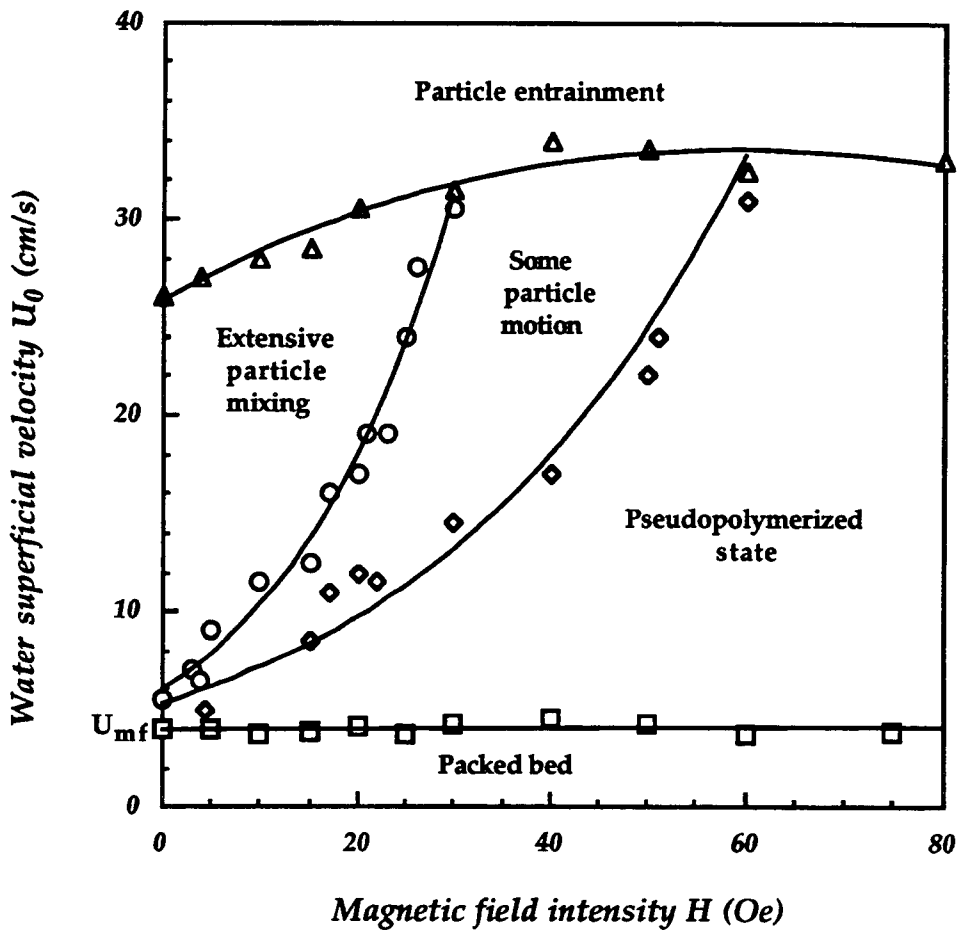

Table 5-1: Fluidization regimes terminology

Equivalent terminology for Kirko and Filippov (1960) definition	Packed bed	Pseudopolymerized State	Particle motion regime	Extensive particle mixing regime
Kwauk et al. (1992)	Fixed bed	Magnetic condensation regime	Chain regime	Particulate regime
Siegell (1987)	Unfluidized bed	Frozen bed or Stabilized regime or Stable regime	Roll-cell regime	Random motion regime
Jovanovic et al. (1993)	Packed bed	Stabilized regime	Partially stabilized regime	Free fluidization state
This study	Packed bed	Stabilized regime	Partially stabilized regime	Random motion regime

Figure 5-2: Typical phase diagram for MSFBs

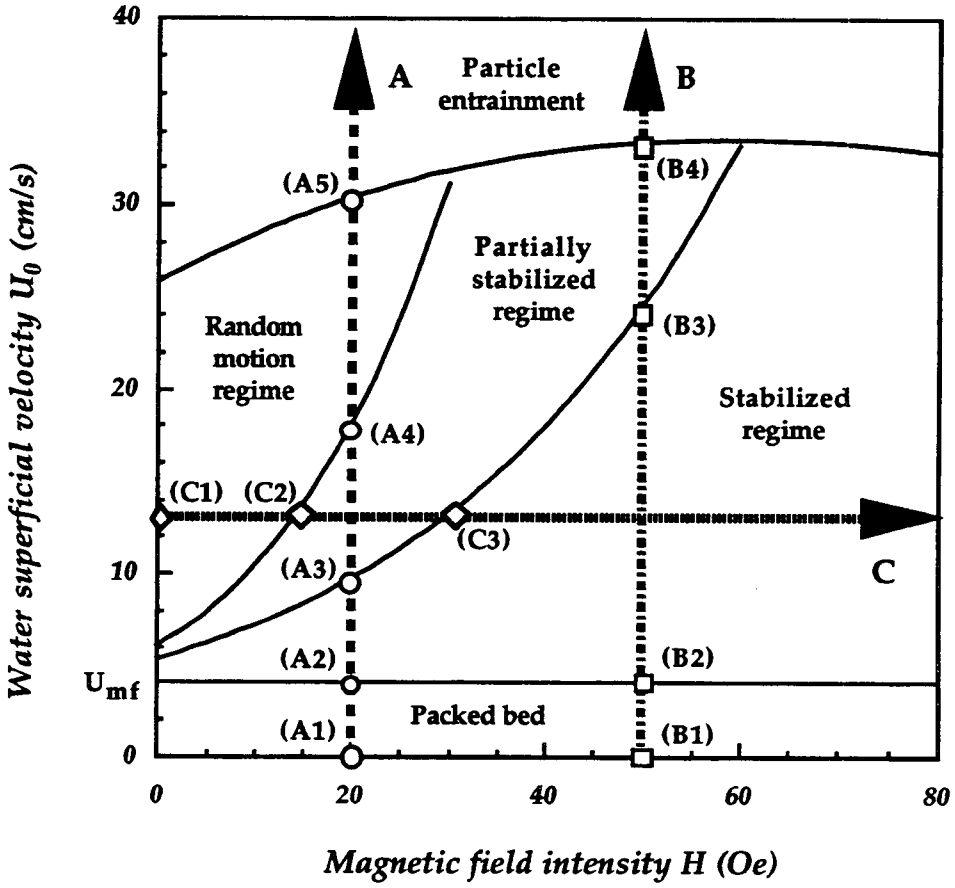

2 - stabilized regime (between points A2 and A3): it begins at the minimum fluidization conditions (point A2). In this regime, particles are immobile. They form extensive chains,

3 - if the fluid velocity is increased (between points A3 and A4), particles at the top of the bed become mobile (point A3). With further increase in the fluid velocity, motion of particles progressively extends downward through the bed. A fluidized state is being developed. The region between points A3 and A4 is called the partially stabilized regime,

4 - for still higher velocities (between points A4 and A5), motion of particles reach the bottom of the bed (point A4). The bed becomes entirely fluidized. Extensive particle motion is observed. The region between points A4 and A5 is called the random motion regime,

5 - if the velocity is further increased, the particle terminal velocity is reached and particles entrainment starts from the top of the bed (point A5).

Following arrow B in Figure 5-2 for a fixed higher magnetic field intensity and increasing fluid velocity, the fluidized bed goes through four different fluidization regimes:

1 - the packed bed regime (between points B1 and B2),

2 - the stabilized regime (between points B2 and B3),

3 - the partially stabilized regime (between points B3 and B4),

4 - the particles entrainment (point B4).

Following arrow C in Figure 5-2 for a fixed velocity greater than the minimum fluidization velocity but smaller than the particles terminal velocity and increasing magnetic field strength, the bed goes through three different regimes:

1 - the random motion regime (between points C1 and C2),

2 - the partially stabilized regime (between points C2 and C3),

3 - the stabilized regime (beyond point C3).

In the random motion regime, obtained within the range of low magnetic field intensities, individual particles are free to move. Turbulent random motion of particles inspired Siegell (1987) to name this regime "random motion" regime. The bed behavior is characterized by a high fluidity of solids.

At the transition between the random motion and the partially stabilized regimes, Siegell (1987) defined a roll-cell region. This region is identified by characteristic motion of particles very often refered to as gulf-streaming.

In the partially stabilized regime, particles form doublets, triplets and other short-chain structures which align themselves with the magnetic flux lines. The bed appears to be quiescent and has a moderate fluidity. However, if the magnetic field intensity is increased, the bed fluidity decreases (Siegell, 1988). Chains grow in length and interact laterally to form intermeshed structures. Intermeshing of chains is generally accompanied by frequent spouts formation described by Kwauk et al. (1992). The transition between partially stabilized and stabilized regimes is very often characterized by these spouts.

In the stabilized regime, the magnetic field is strong enough to close the spouts. An overall loose structure consisting of vertically oriented sessile chains is

established. The particles are frozen (Siegell, 1988), forming an immobile mass which is no longer fluidized. The bed has totally lost its fluidity.

The regime map identifies different fluidization regimes, each characterized by particular behaviour of particles in MSFBs and is often refered to as "phase diagram". Sonolikar (1989) and Liu et al. (1991) illustrated the analogy between the regime map and the thermodynamic properties appearing in a traditional phase diagram. The ordinate of the regime map is the fluid velocity, analogous of the thermodynamic temperature. The abscissa of the regime map is the magnetic field intensity and is analog of the thermodynamic pressure. The packed bed region is analog of the solid phase. The stabilized and partially stabilized regimes correspond to the liquid phase. The random motion regime corresponds to the thermodynamic vapor state.

5.2 - Overall pressure drop through the bed and minimum fluidization velocity

In a conventional bed, particles are subject to three macroscopic forces: the gravitational force F_g, the drag force F_d, the buoyancy force F_b. As the fluid velocity through the bed increases, the drag force exerted on the particles increases and the pressure drop, which is a measure of this drag force, increases as long as the bed is unfluidized. As soon as the drag force balances the other forces, the bed becomes fluidized ($U_0 = U_{mf}$). In a conventional bed:

$$F_d = F_g - F_b = \frac{\pi d_p^3}{6} (\rho_p - \rho) g \qquad \text{(Eq. 5-1)}$$

With further increases in the fluid velocity, the drag force remains constant. The pressure drop is sufficient to support the weight of particles and therefore remains constant (Figure 5-3).

In a MSFB, it is known that a uniform field does not create any net force within the MSFB. Rosensweig (1979 b) showed that the magnetic force is proportional to the gradient of the magnetic field. In a uniform field, this gradient is null. Therefore, the net force on the bed of particles is zero.

Filippov (1960) and Siegell (1987) reported that the pressure drop in a magnetic fluidized bed is also equal to the weight of the bed, just as in the absence of magnetic field. However, they observed that the presence of a magnetic field causes the bed height to decrease. They explained the constant value of the pressure drop by the formation of a more ordered, structured bed in which channels of lower resistance are formed, allowing the fluid to flow at a higher flow rate (Figure 5-4).

Ivanov and Grozev (1970) reported that the bed resistance to fluid flow is increasing with an increase of the magnetic field intensity. Hence, they proposed that the effect of the field can be viewed as an additional weight on the bed. However, this is in contradiction with the work of Filippov (1960), Rosensweig (1979 a, 1979 b) and Siegell (1987) and most of the recent studies. It seems that their magnetic field was not uniform so that existing field gradients could induce an additional force on the bed.

Bologa and Syutkin (1977) reported a decrease in the bed pressure drop as magnetic field strength is increased. They concluded that this behavior was a result of an ever increasing order of the structure of the MSFB. Channels which are formed in the bed offer less resistance to fluid flow.

Figure 5-3: Fluidization curve for a conventional bed

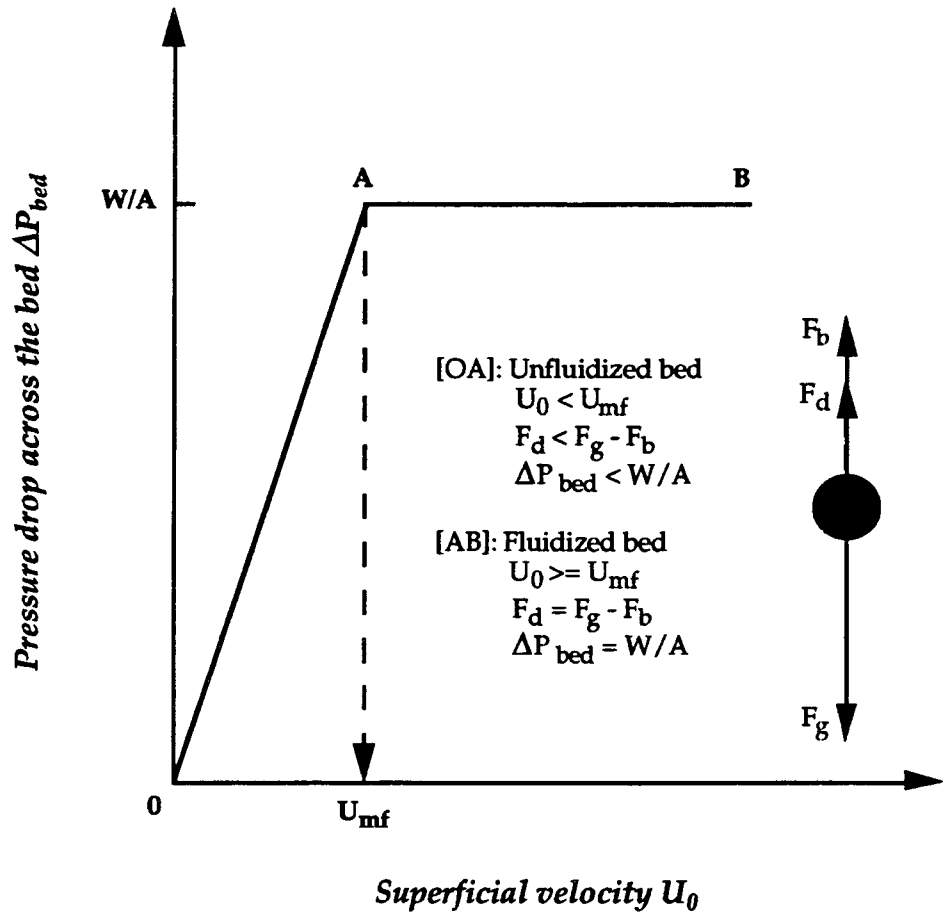

Figure 5-4: Particles arrangement in a MSFB (Arnaldos et al., 1985)

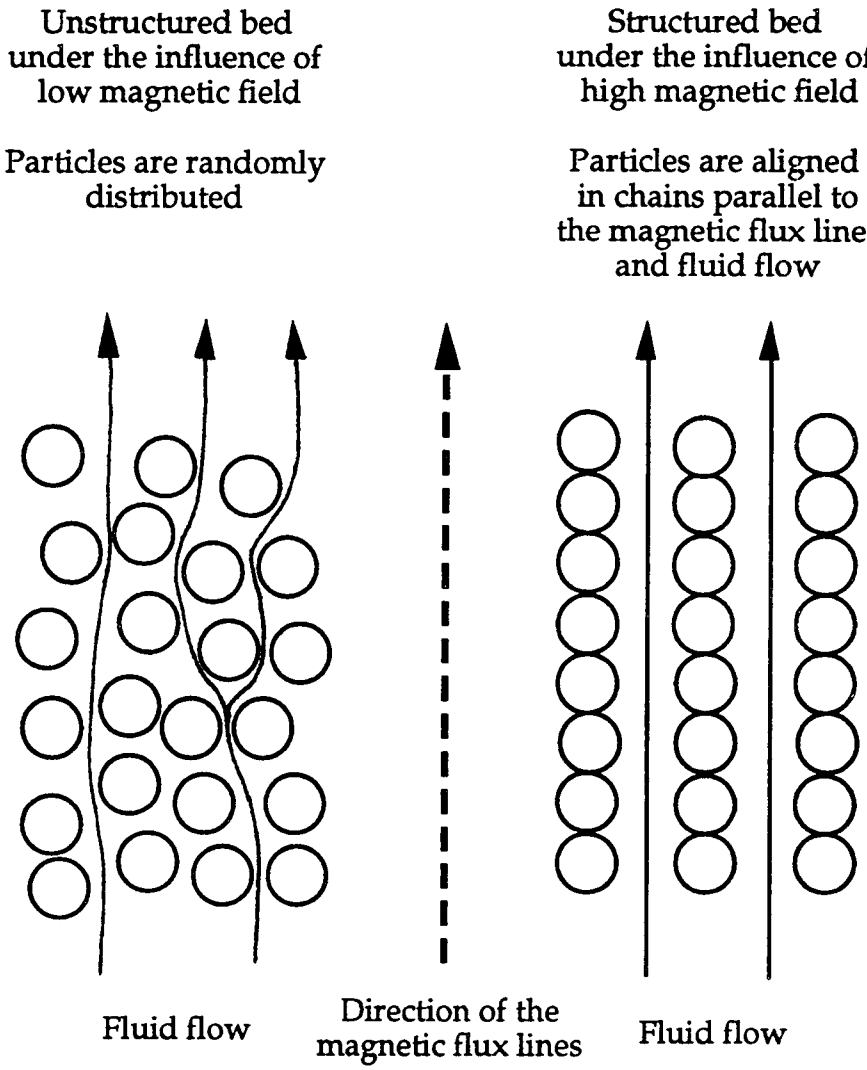

Rosensweig (1979 a) reported a constant pressure drop in MSFBs for different magnetic field intensities. He also reported that the slope of the initial part of the fluidization curve (segment [OA] in Figure 5-3) is independent of the field strength and can be predicted by the Ergun equation (Kunii and Levenspiel, 1991):

$$\frac{\Delta P_{bed}}{L} g_c = 150 \frac{(1-\varepsilon)^2}{\varepsilon^3} \frac{\mu U_0}{(\Phi_s d_p)^2} + 1.75 \frac{1-\varepsilon}{\varepsilon^3} \frac{\rho U_0^2}{\Phi_s d_p} \qquad \text{(Eq. 5-2)}$$

This behavior is common to a conventional bed and the value of U_{mf} is therefore independent of the magnetic field.

Contrary to this, Bologa and Syutkin (1977), reported that the minimum fluidization velocity rises when the field intensity is increased. Unfortunately, they did not report their experimental conditions and they did not show any fluidization curve.

Sonolikar et al. (1972) defined U_{mf} as the onset of agitation of particles in the bed and asserted that the relationship between U_{mf} and H is exponential. However they presented no fluidization curve which may allow comparison between visual observations and ΔP_{bed} variations with fluid velocity. Jovanovic and Jovanovic (1993) described similar bed properties. Thus defined minimum fluidization velocity corresponds to the transition velocity between the stabilized and the partially stabilized regimes.

With increasing field intensity, the bed behavior changes due to the interaction forces between the particles (Penchev and Hristov, 1990). The induced magnetic forces are of cohesive nature and often become dominant forces in the system. Also with increasing velocity, the bed continuously changes its structure in such a way as to offer minimum hydraulic resistance. The chain structure has low

resistance and high mechanical stability since the strings are collinear to the field and the flow.

5.3 - Average bed porosity

Bakker and Heertjes (1958, 1960) characterized three different zones in a fluidized bed based on the bed porosity. The first zone, Zone 1, extends upward from the distributor plate; its length mainly depends on the distributor characteristics. Zone 2 is a middle layer. Porosity in this layer is fairly homogeneous. Zone 3, at the top of the bed, has a larger porosity. This is similar to what was previously shown in Figures 4-1 and 4-3. Shumkov and Ivanov (1975, 1977) found that at fixed velocity, with increasing field, the length of the constant porosity zone, Zone 2, increases at the expense of Zone 3. The applied magnetic field tends to make the bed more uniform in porosity.

Filippov (1960) reported that the initial expansion of MSFB is independent of magnetic field strength.

Kwauk et al. (1992) are among the few who published data for the porosity in a magnetically stabilized liquid-solid fluidized bed. They reported the change in bed porosity for different fluidization regimes. One can summarize their findings as follows:

1 - in the random motion regime, the bed voidage is little affected by the magnetic field,
2- in the partially stabilized regime, there is a continuous reduction in bed voidage with increasing field strength,

3- in the stabilized regime, when a frozen bed is formed, the porosity is essentially constant. The field intensity has no influence on the bed porosity.

Kwauk et al. (1992) presented an equation for the prediction of porosity as a function of magnetic field intensity and other characteristic parameters of the system:

$$\frac{\varepsilon - \varepsilon_M}{\varepsilon_P - \varepsilon_M} = \exp\left[\left(\frac{H}{H_0}\right)^s\right] \qquad \text{(Eq. 5-3)}$$

According to their work, the ε - H curves at constant liquid flow rate show a S-shape that could be divided into three parts: the random motion, partially stabilized, and stabilized regimes as shown in Figure 5-5.

More recently Jovanovic and coworkers (1993) transformed Equation 5-3 to correlate their expansion data in a liquid-solid fluidized bed. They defined the void function V_ε as follows:

$$V_\varepsilon = \frac{\varepsilon - \varepsilon_{ms}}{\varepsilon_{ff} - \varepsilon_{ms}} = e^{-a H} \qquad \text{(Eq. 5-4)}$$

where ε_{ff} is the bed porosity in free fluidization regime (H = 0) and ε_{ms} is the bed porosity at transition between the partially stabilized regime and the stabilized regime (minimum stabilization conditions).

Working on gas-solid magnetically stabilized fluidized beds, Arnaldos et al. (1985) suggested the use of the bed voidage function $\frac{\varepsilon^3}{1-\varepsilon}$ to characterize the change in porosity with magnetic field intensity. However, their paper does not give any correlated data.

Figure 5-5: Porosity versus field strength curve
from Kwauk et al. (1992)

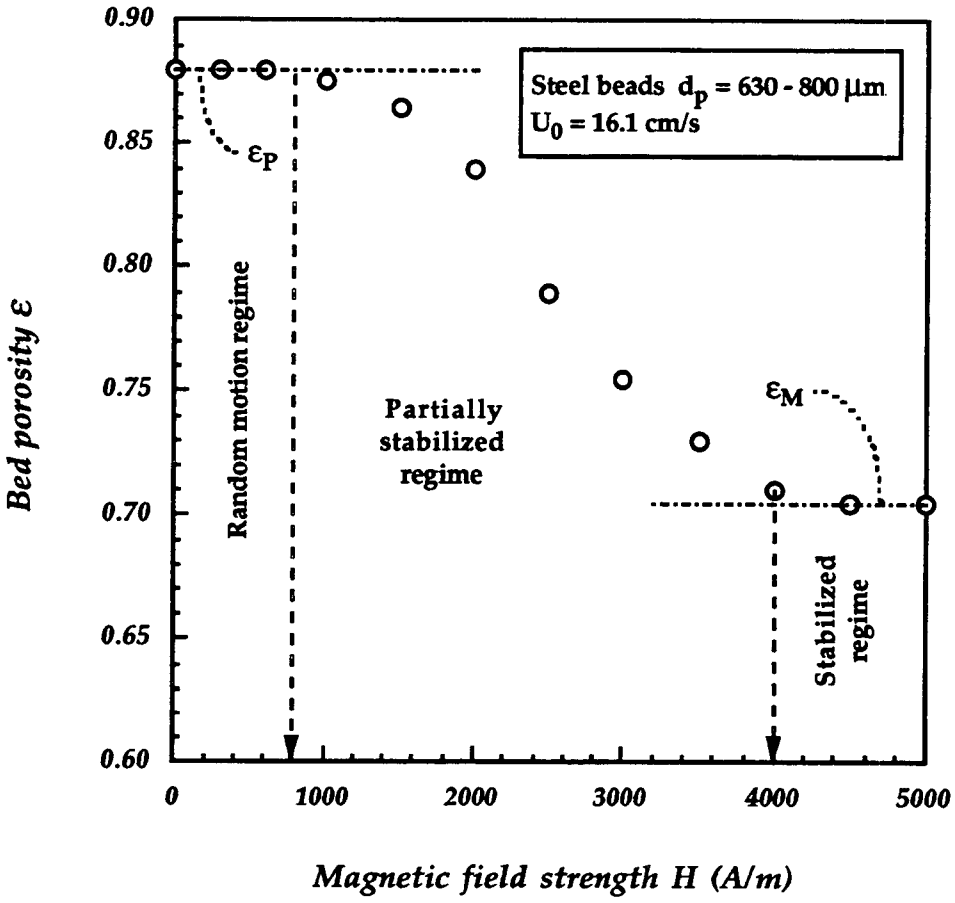

5.4 - Discussion

All previous investigators came to very similar conclusions as to the behaviour of MSFBs. Even though they named differently the fluidization regimes, their phase diagrams are equivalent.

Few correlations were given to predict the change in average bed porosity in MSFBs. The model developed by Jovanovic et al. (1993) has similar features to the correlation given by Kwauk et al. (1992), but both models are applicable only for particular particles. Magnetic properties of the particles have rarely been taken into account, and no attempt has been made to find a generalized correlation.

CHAPTER 6
EXPERIMENTAL RESULTS AND DISCUSSION

The experiments conducted for this study allow us to discuss three different points. We focus our attention on the regime maps developed for both types of particles (A and B), on the changes in the pressure drop and average bed porosity, both as functions of water superficial velocity and magnetic field intensity.

We propose an equation for the change in the transition velocity between the stabilized regime and the partially stabilized regime (U_{ms}) as a function of the magnetic field intensity at this transition (H_{ms}). We also found a correlation for the change in the porosity at this same transition (ε_{ms}) as a function of U_{ms}. Finally, we developed a model for the prediction of the average bed porosity for a given water velocity and magnetic field intensity.

6.1 - Maps of fluidization regimes in MSFBs

The regime maps obtained from experiments are displayed in Figures 6-1 and 6-2 for particles A and B respectively. There was no difference in the maps whether the bed was fluidized in the "magnetization first" mode or in the "fluidization first" mode.

Figure 6-1: Experimental map of fluidization regimes for particles A

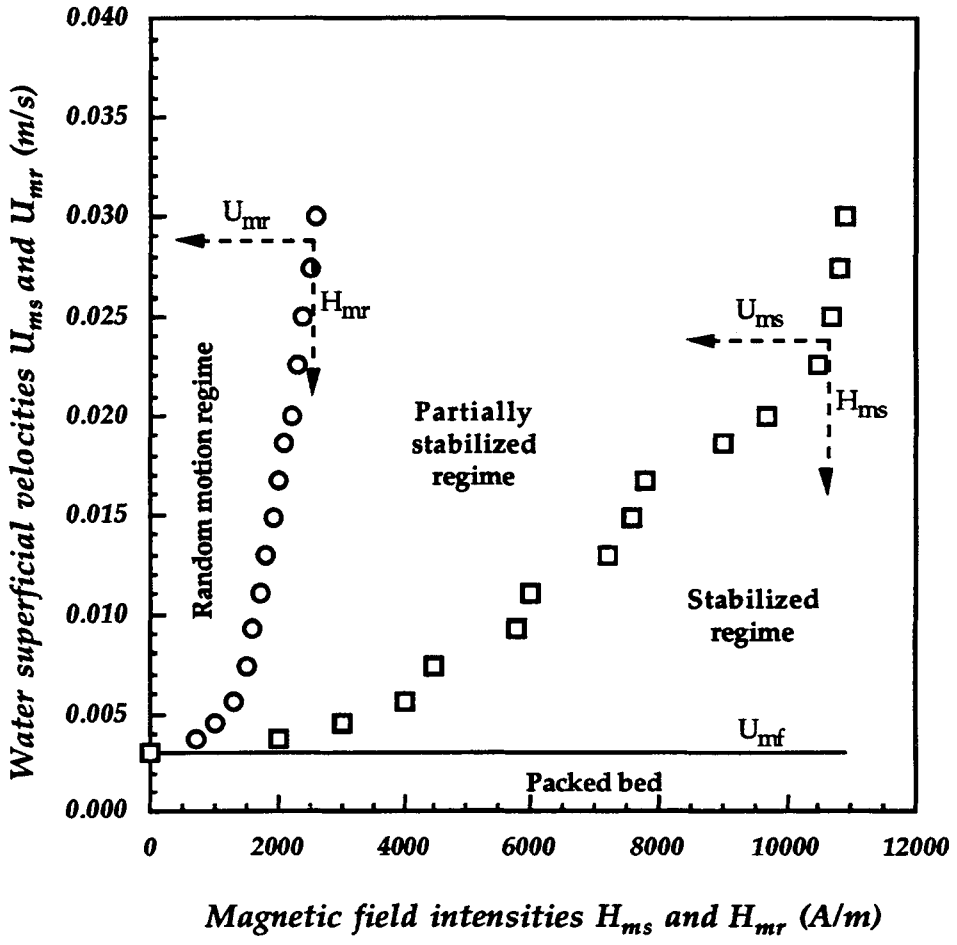

Figure 6-2: Experimental map of fluidization regimes for particles B

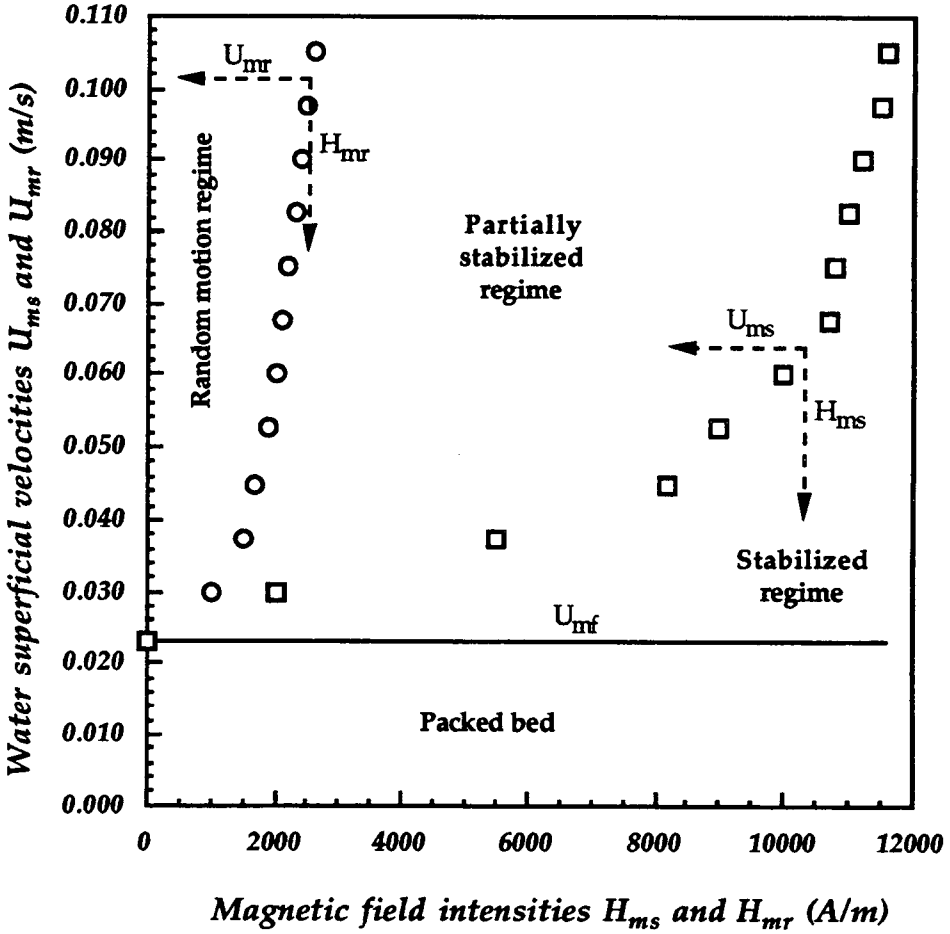

These regime maps are analogous of the one reported by Kwauk et al. (1992) and are composed of three different regimes:

1 - the packed bed regime,

2 - the stabilized regime,

3 - the partially stabilized regime,

4 - the random motion regime.

We did not exceed particles terminal velocities so that we did not loose particles and the weight of the bed remained constant. Therefore, the particle entrainment regime does not appear on our diagrams.

Below the minimum fluidization velocity, the bed is packed. The structure of the bed remains unchanged in the presence of a magnetic field.

In the stabilized regime, particles are still immobile for a velocity greater than the minimum fluidization velocity U_{mf}. This state extends until $U_0 = U_{ms}$, where U_{ms} is the fluid velocity at which the partially stabilized regime starts.

For a constant field intensity, as the velocity is increased beyond U_{ms}, particles align in a direction parallel to the flow and to the magnetic field lines. This regime of fluidization is designated as partially stabilized regime after Jovanovic et al. (1993) and extends until $U_0 = U_{mr}$. U_{mr} is the fluid velocity at which the minimum conditions for the random motion regime to occur are met.

In the random motion, the magnetic field is too weak to restrict the particles motion. The bed has the same appearance as in the absence of magnetic field. However, the bed porosity is somewhat influenced by the magnetic field.

The transition velocities U_{ms} and U_{mr} were determined by visual observations as well as by bed porosity measurements (see Section 6.3 of this Chapter). The results agree quite well.

The fluidization mode was found to have no influence on the regime map, that is to say on the determination of U_{ms} and U_{mr}. This is in agreement with the observations by Siegell (1987).

From Figures 6-1 and 6-2, we see that both transition velocities U_{ms} and U_{mr} increase with increasing magnetic field strength. This agrees with the fact that the bed becomes more and more structured when the magnetic field intensity is increased, hence delaying the transition between the different fluidization regimes.

In this study, an experimental correlation between U_{ms} and H_{ms} is given, where H_{ms} is the magnetic field needed to reach the transition between the partially stabilized regime and the stabilized regime for a fixed fluidization velocity $U_0 = U_{ms}$ (Figures 6-1 and 6-2):

$$\frac{U_0}{U_{mf}} M_{ms} = \frac{U_{ms}}{U_{mf}} M_{ms} = b \left[e^{c H_{ms}} - 1 \right] \qquad \text{(Eq. 6-1)}$$

or

$$\frac{U_0}{U_{mf}} = \frac{U_{ms}}{U_{mf}} = \frac{b}{M_{ms}} \left[e^{c H_{ms}} - 1 \right] \qquad \text{(Eq. 6-2)}$$

where

$$M_{ms} = (\alpha H_{ms} + \beta) H_{ms} \qquad \text{(Eq. 6-3)}$$

This correlation is valid for $U_0 \geq U_{mf}$ and will be used later (Section 6.3 of this Chapter) for the prediction of the average bed porosity at different velocities and

magnetic field intensities. The term M_{ms} is the magnetization intensity of the particles. Coefficients α and β are reported in Table 2-1 as characteristic properties of the particles. b and c are experimental correlation parameters found by fitting the experimental data points by the Least Squares Method as described in Appendix D. We obtain:

1 - for particles A:

$$\frac{U_0}{U_{mf}} M_{ms} = \frac{U_{ms}}{U_{mf}} M_{ms} = 2253 \left[e^{4.373\,10^{-4} H_{ms}} - 1 \right] \qquad \text{(Eq. 6-4)}$$

2 - for particles B:

$$\frac{U_0}{U_{mf}} M_{ms} = \frac{U_{ms}}{U_{mf}} M_{ms} = 9510 \left[e^{3.20510^{-4} H_{ms}} - 1 \right] \qquad \text{(Eq. 6-5)}$$

Values predicted by Equations 6-4 and 6-5 and experimental data are plotted in Figure 6-3.

We strongly believe that coefficients b and c are function of particles characteristics as well as vessel and distributor plate characteristics. This was suggested by Siegell (1987) who obtained different values for the transition velocity between the stabilized and the partially stabilized regimes when using two different distributors.

We think that it is reasonable to assume that the distributor plate characteristics influence the transition velocity from stabilized to partially stabilized regimes. When particles in the bed align themselves in chains, they sit on top of each other. At the bottom of the chain, particles sit on the distributor plate as shown in Figure 6-4. The velocity of the water coming out of the distributor orifices is very high, and water flows in small jets for some distance above the distributor.

Figure 6-3: U_{ms} versus H_{ms} model fit

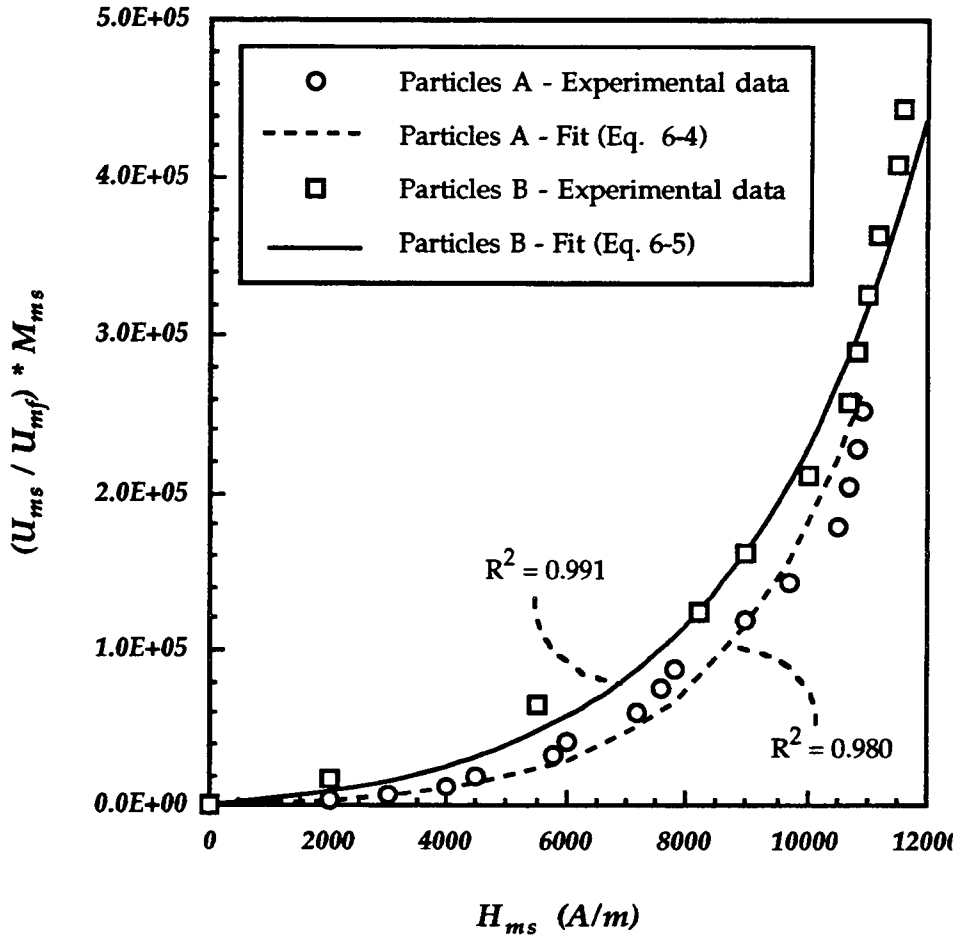

Figure 6-4: Effects of the distributor and the water jets on the stabilized bed structure

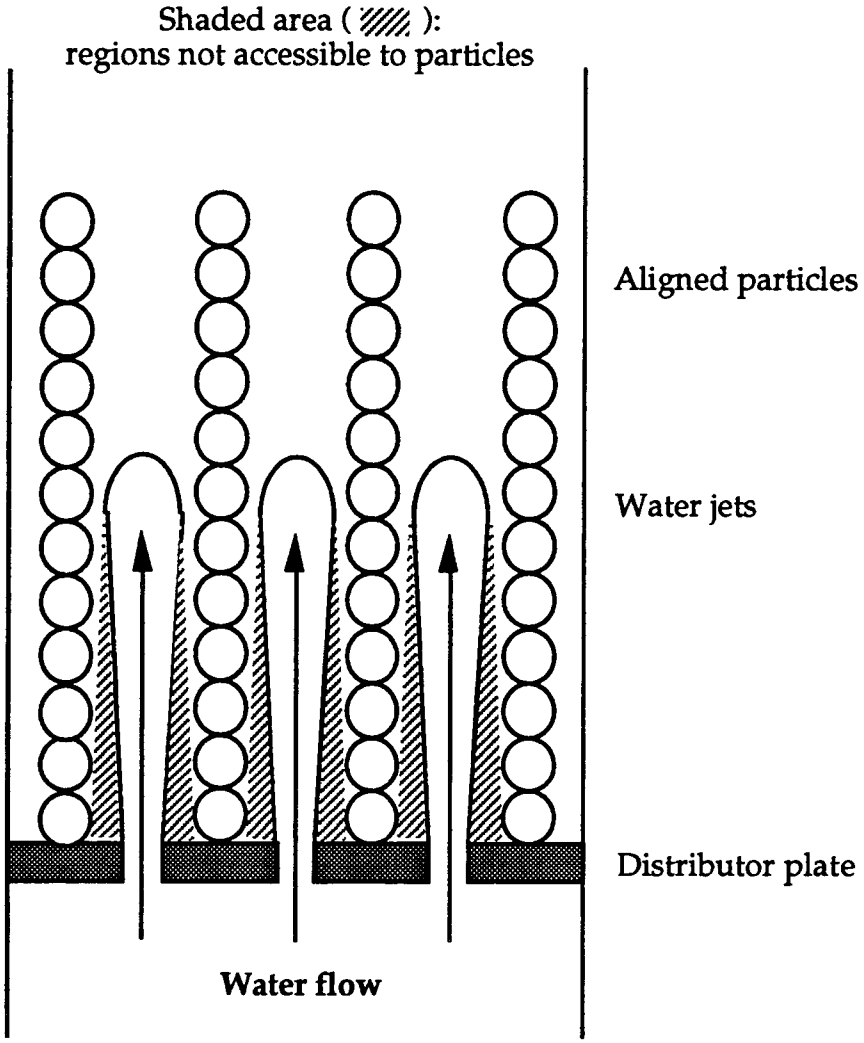

Water jets exchange momentum with surrounding water and particles. These jets do not allow particles to sit on the distributor holes. This is pictured in Figure 6-4. Hence, the structure of the bed depends on the distributor configuration which in turn affects the transition velocity from stabilized to partially stabilized regimes.

To accurately predict parameters b and c, more studies are needed. By collecting data for different distributors and different particles, one could eventually determine the influence of their respective characteristics.

6.2 - Overall pressure drop through the bed

Data for the overall pressure drop across the bed were obtained from experiments as described in Chapter 4. Figures 6-5 and 6-6 display ΔP_{bed} as a function of water superficial velocity for constant magnetic field intensities, for particle types A and B, respectively. Figures 6-7 and 6-8 show ΔP_{bed} as a function of magnetic field intensity for constant water superficial velocity, for particles A and B respectively. No difference was found for the pressure drop data whether the bed was fluidized in the "magnetization first" mode or in the "fluidization first" mode.

From these four graphs, we see that:

1 - for H = 0, the pressure drop becomes constant when the bed is fluidized. The bed behaves in the random motion regime and the pressure drop is equal to the weight of particles per unit area,

Figure 6-5: Overall pressure drop across the bed versus water superficial velocity for constant magnetic field intensities for particles A

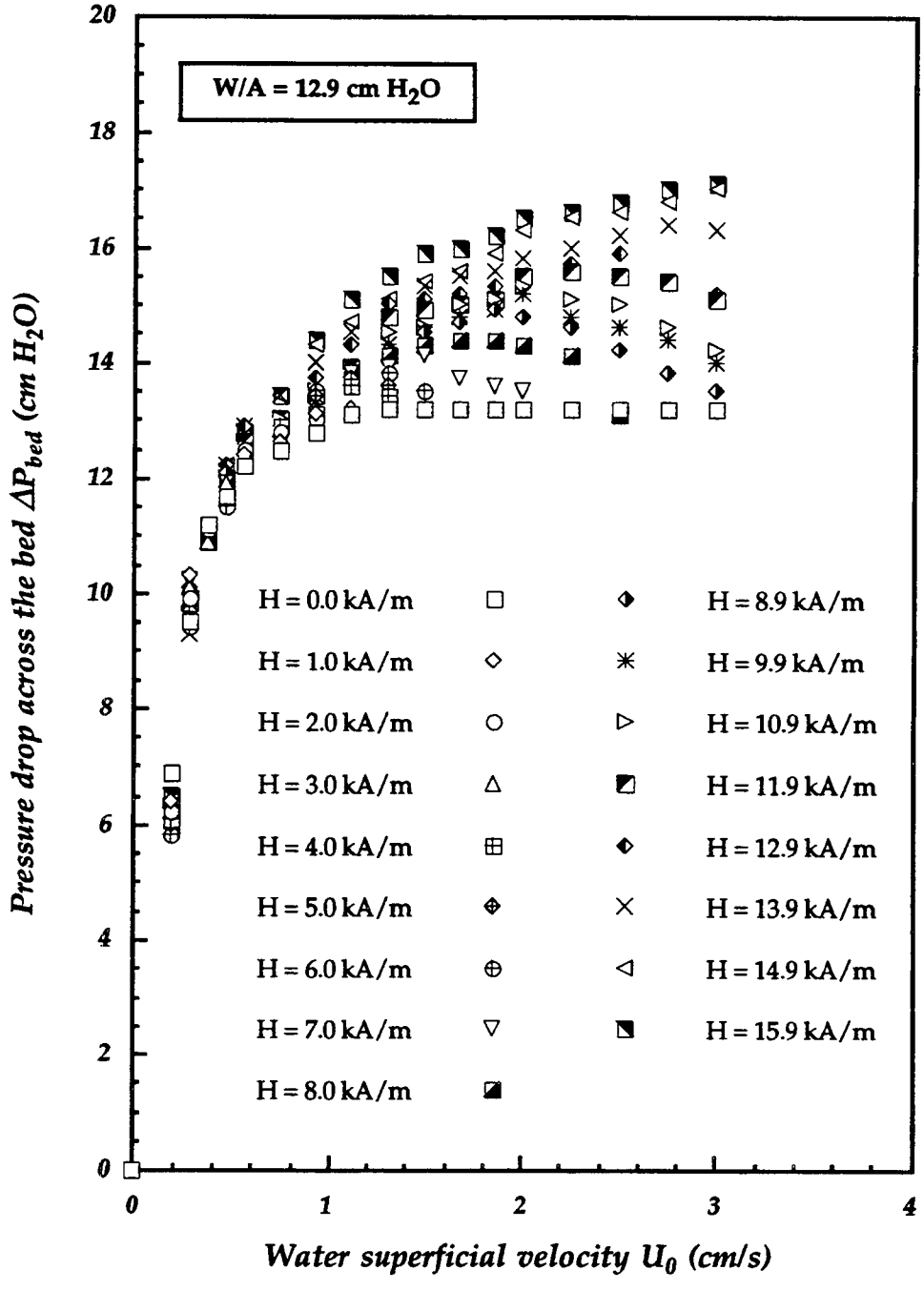

Figure 6-6: Overall pressure drop across the bed versus water superficial velocity for constant magnetic field intensities for particles B

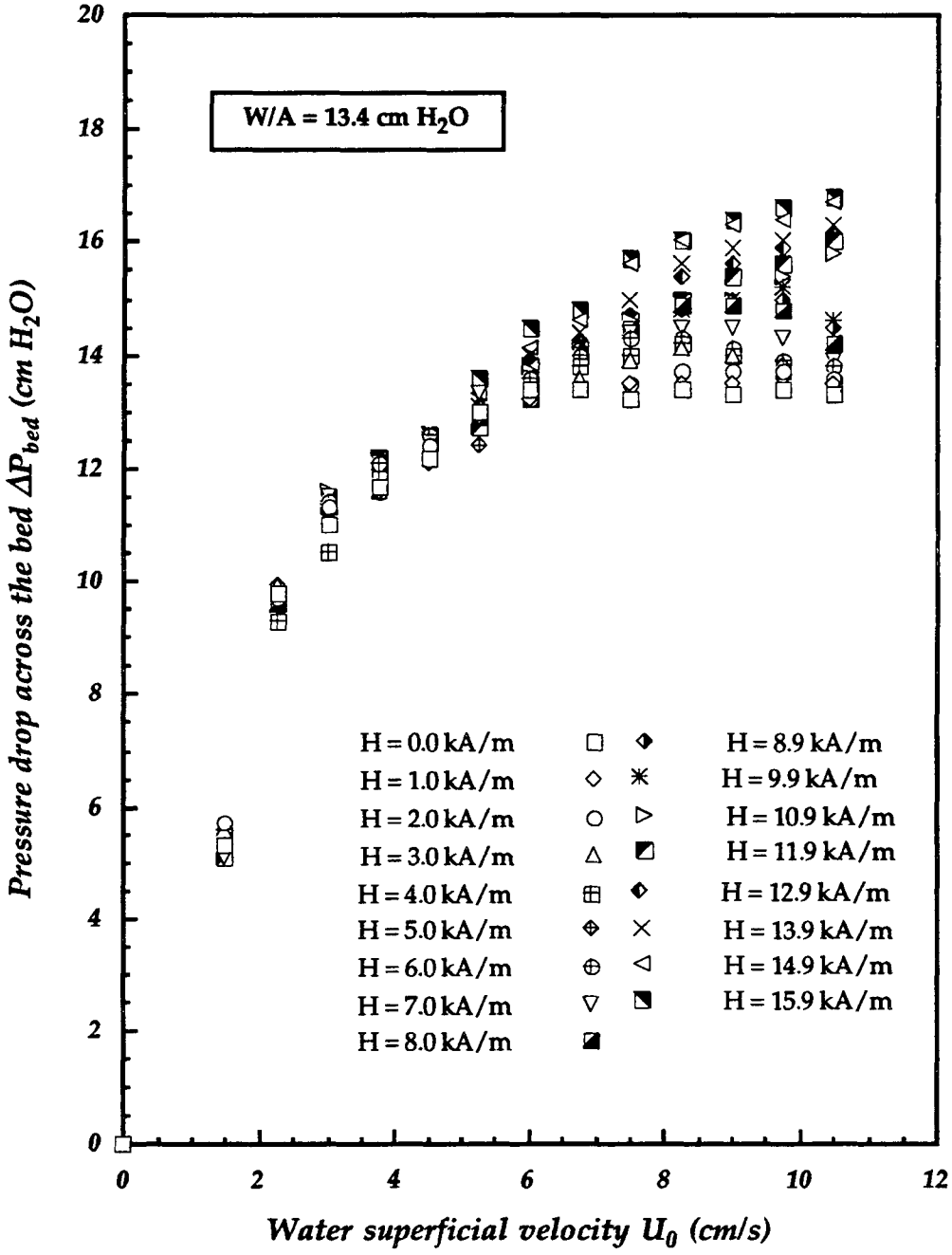

Figure 6-7: Overall pressure drop across the bed versus magnetic field intensity for constant water superficial velocities for particles A

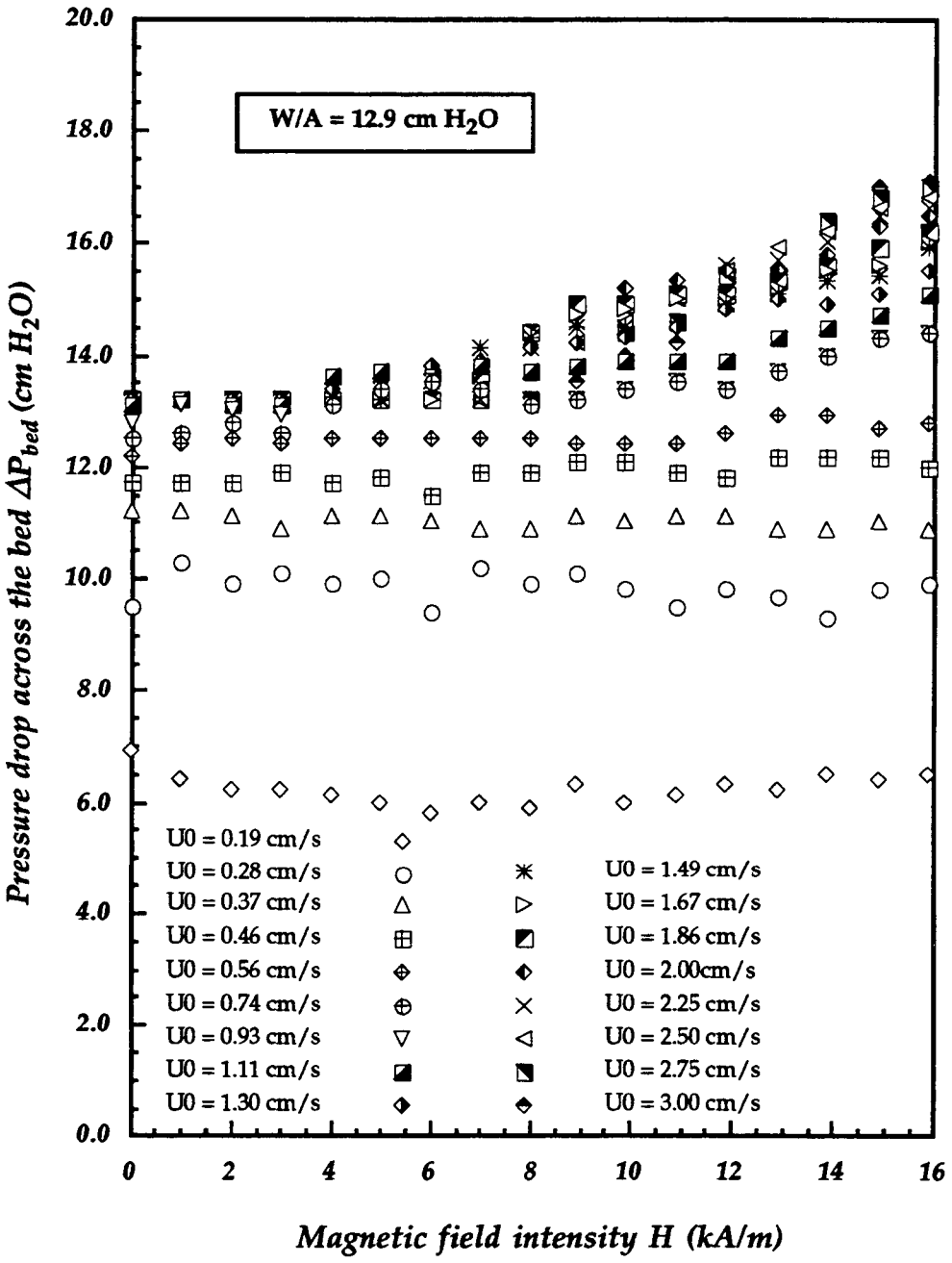

Figure 6-8: Overall pressure drop across the bed versus magnetic field intensity for constant water superficial velocities for particles B

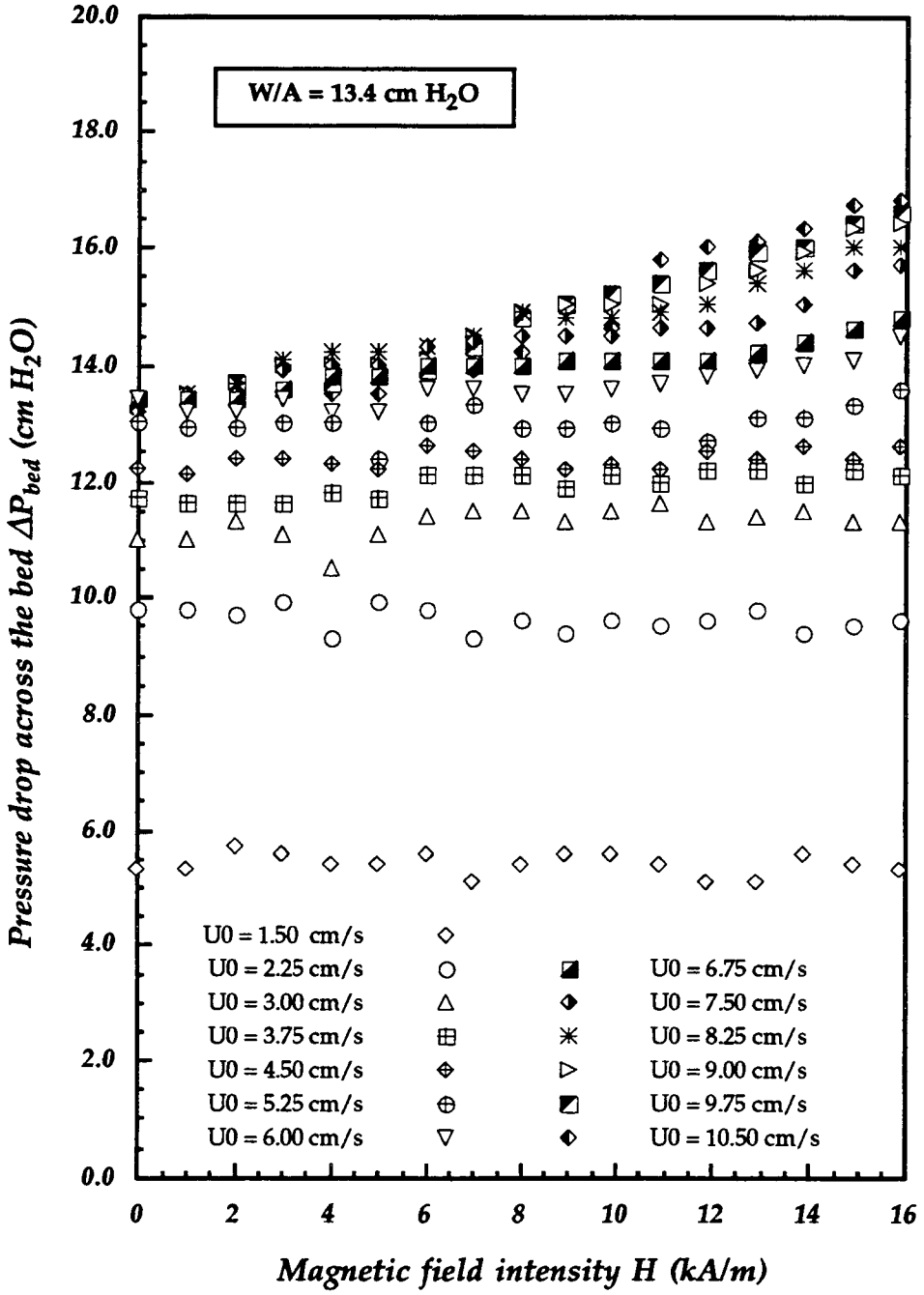

2 - for a given magnetic field intensity, when velocity is increased, the bed goes through the packed bed regime, then through the stabilized regime with an increase in the pressure drop above the weight of the particles per unit area until U_{ms} is reached. In the partially stabilized regime, for $U_{ms} \leq U_0 \leq U_{mr}$, the pressure drop decreases as U_0 increases. Finally, in the random motion regime, the pressure drop is constant, equal to the weight of the particles per unit area,

3 - for a given velocity $U_0 < U_{mf}$, the pressure drop in the packed bed is independent of the magnetic field intensity. Its value is lower than the weight of particles per unit area. When $U_0 \geq U_{mf}$, the bed is fluidized and the pressure drop is constant, equal to the particles weight when the bed is operated in the random motion regime. When magnetic field strength is high enough to reach the onset of the partially stabilized regime, the pressure drop begins to increase beyond the particles weight. As the field intensity is further increased, the pressure drop increases throughout the partially stabilized regime and the stabilized regime.

The fact that the pressure drop was found to increase in an increasing uniform magnetic field strength is in contradiction with previous studies (Filippov, 1960; Siegell, 1987). However, this can be explained by the following.

The pressure drop through a fluidized bed is a function of the drag coefficient of the fluid on the solids and of the fluid velocity. The drag coefficient itself is a function of the particles characteristics and the fluid velocity (Equation 2-5). For a constant velocity, changes in ΔP_{bed} are due to changes in the drag coefficient, C_D. When the bed undergoes restructuration because of the influence of the magnetic field, particles attach to each other. They do not behave discretely any

more. The drag coefficient of agglomerated particles is smaller than that of a single particle. Therefore particles tend to defluidize and "sink" toward the distributor plate. This phenomenon can be the cause of a decrease in pressure drop through the bed. Defluidized magnetized particles accumulate at the bottom of the bed. Then, they behave like a magnet, attracting particles from the upper part of the bed. This may be viewed as creating an additional net force on the particles. This force on particles is directed toward the bottom of the bed, and may be responsible for an increase in the overall pressure drop through the bed. We must also consider the momentum exchange between the defluidized particles and the vessel walls. As particles agglomerate at the bottom of the bed, an increase in the magnetic field strength at a constant fluid velocity reduces the bed height, thus compressing the particles down. This is accompanied by a large increase of the friction force between the particles getting more and more structured and the vessel walls. Therefore, we can decompose the overall pressure drop through the bed as:

$$\Delta P_{bed} = \frac{W_f}{A} + \Delta P_m + \Delta P_f \qquad \textbf{(Eq. 6-6)}$$

where $\frac{W_f}{A}$ accounts for the weight of fluidized particles per unit area. ΔP_m is the additional pressure drop due to the magnetic net force acting on the particles attracted toward the bottom of the bed. ΔP_f accounts for the frictional force. It seems reasonable to think that ΔP_m is function of the magnetic properties of the particles and that ΔP_f is function of the fluid flow rate, of the properties of the fluid (i.e. density ρ), of the characteristics of the particles (i.e. d_p) and of the vessel geometry (i.e. D).

6.3 - Average bed porosity

Data for the average bed porosity were obtained from bed height measurements as discussed in Chapter 4. Figures 6-9 and 6-10 show porosity as a function of water superficial velocity for constant magnetic field intensities for both types of particles A and B, respectively. Figures 6-11 and 6-12 show porosity as a function of magnetic field intensity for constant water superficial velocities for A and B particles respectively. No difference was found for the porosity data whether the bed was fluidized in the "magnetization first" mode or in the "fluidization first" mode.

From these four figures, we can see that:

1 - for a given magnetic field strength, the average bed porosity increases when the velocity is increased,
2 - for a given velocity, the average bed porosity decreases when the magnetic field strength is increased.

This is in agreement with previous studies in liquid-solid fluidization (Kirko and Filippov, 1960; Siegell, 1987; Kwauk et al., 1992; Jovanovic et al., 1993).

Figures 6-11 and 6-12 are analogous of the curves reported by Kwauk et al. (1992). From these plots, we can distinguish the four different regimes of fluidization reported in Section 6.1 of this Chapter:

1 - before minimum fluidization velocity is reached, the packed bed porosity is constant, independent of velocity and magnetic field strength,

Figure 6-9: Average bed porosity changes as a function of water superficial velocity for constant magnetic field intensities for particles A

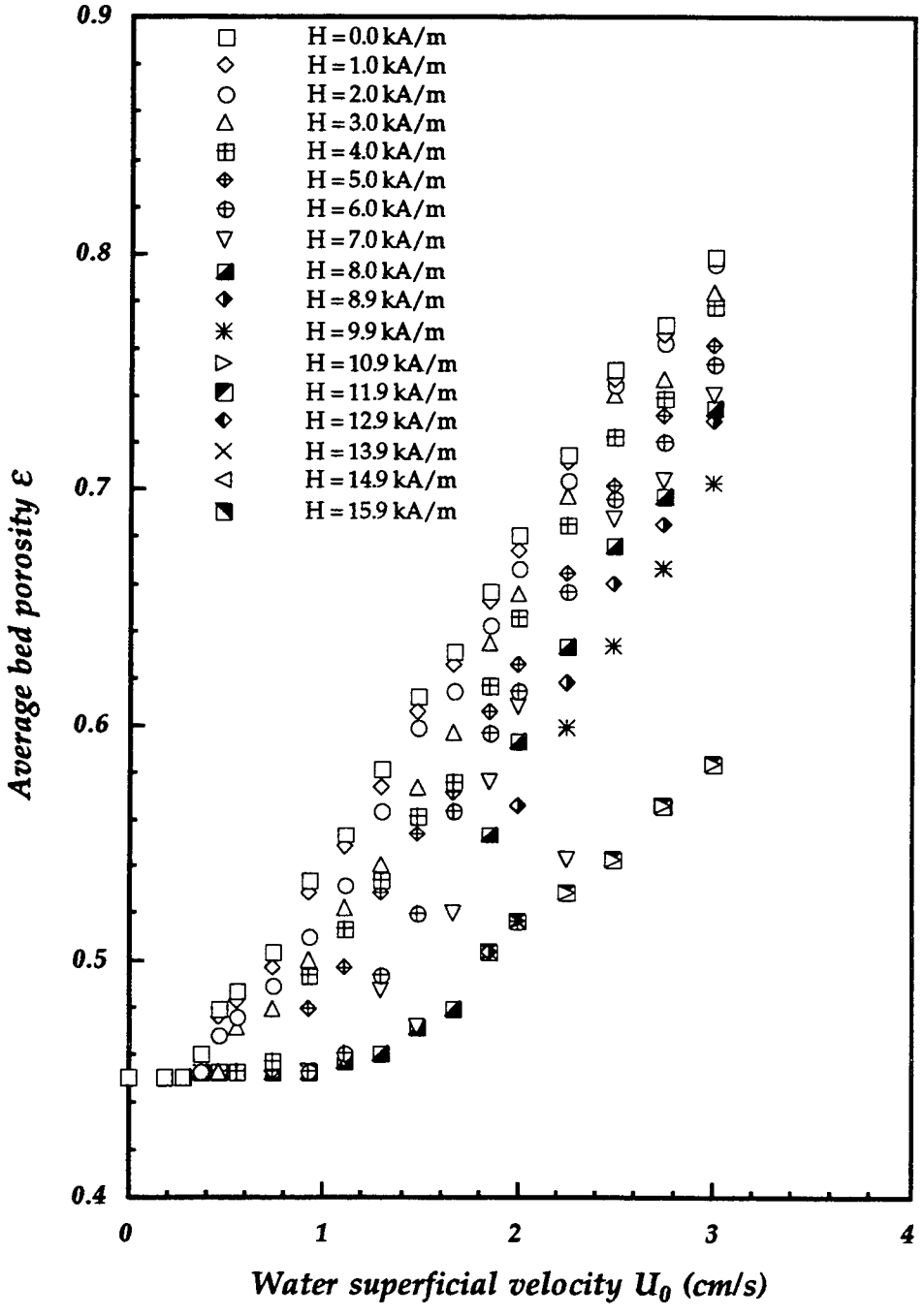

Figure 6-10: Average bed porosity changes as a function of water superficial velocity for constant magnetic field intensities for particles B

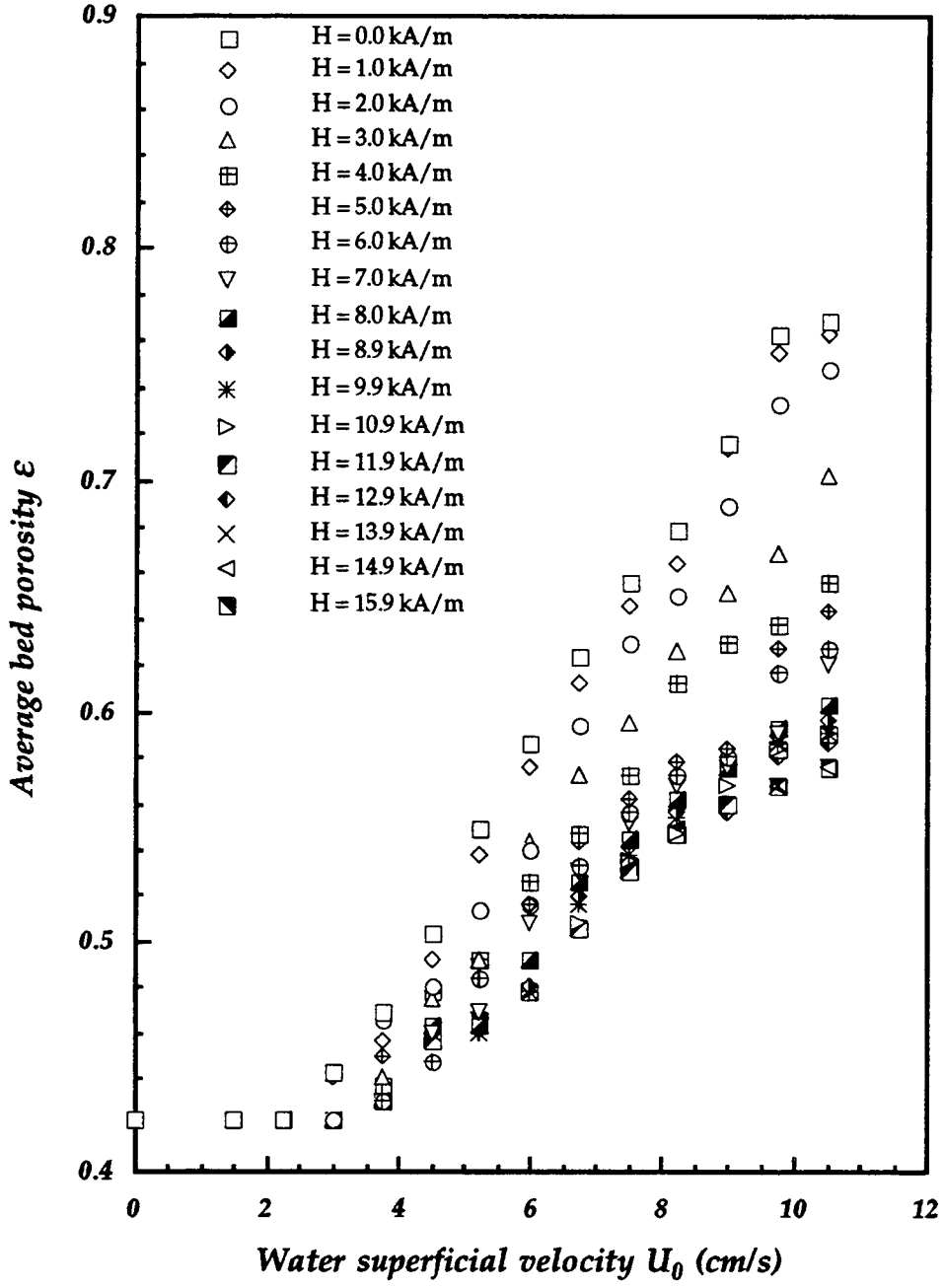

Figure 6-11: Average bed porosity changes as a function of magnetic field intensity for constant water superficial velocities for particles A

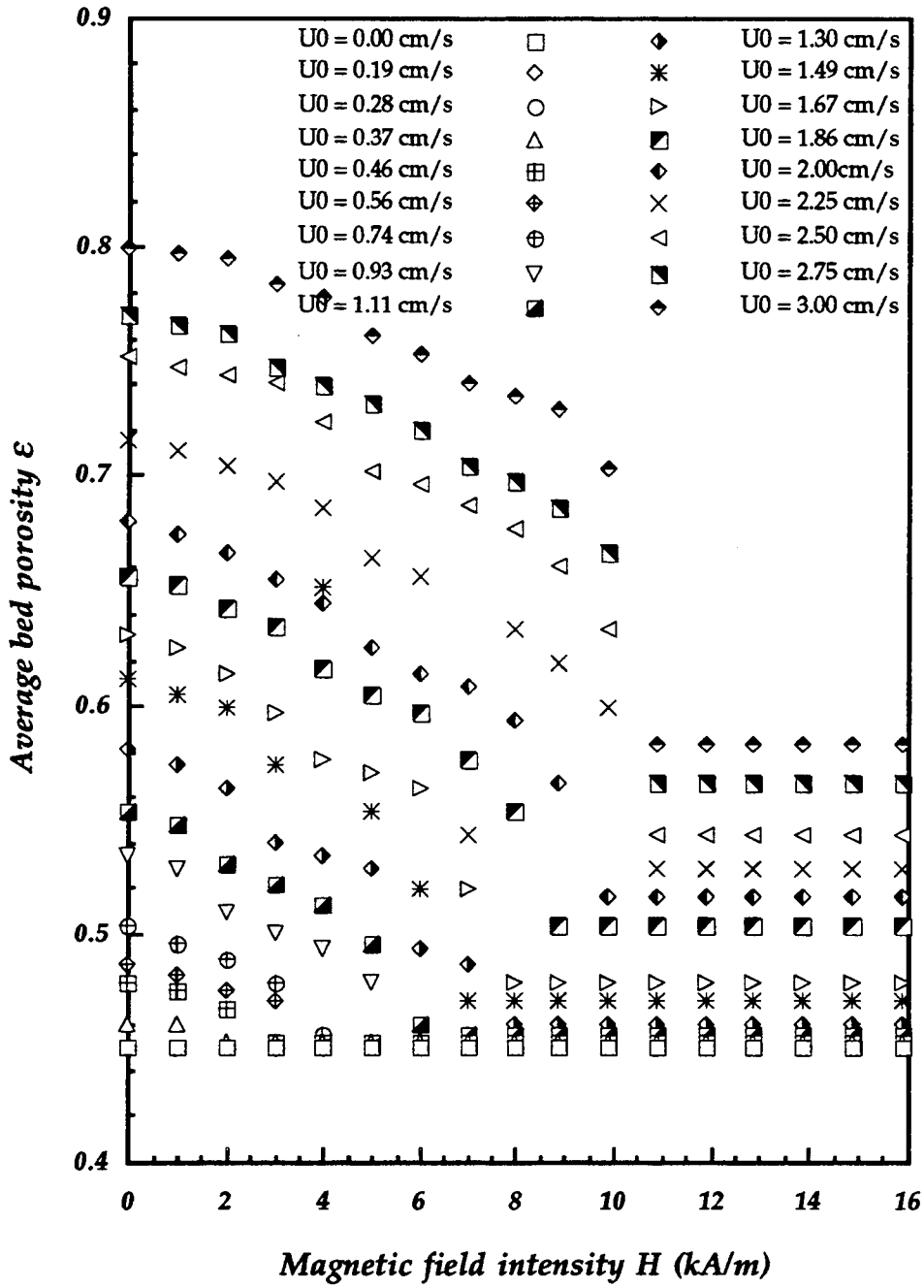

Figure 6-12: Average bed porosity changes as a function of magnetic field intensity for constant water superficial velocities for particles B

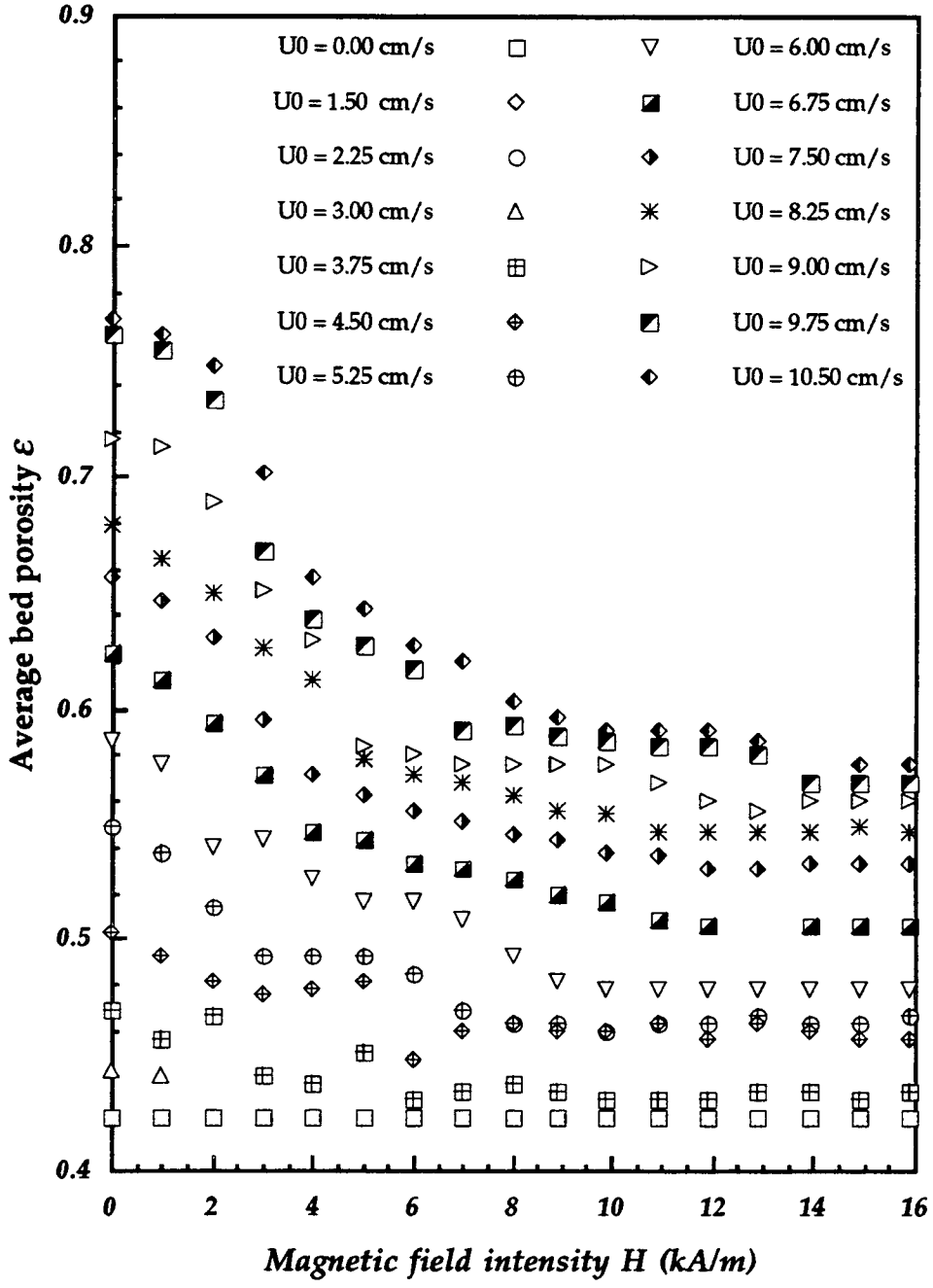

2 - in the stabilized regime, for a given velocity, the porosity is constant, independent of the magnetic field intensity. However, it increases with water velocity,

3 - in the partially stabilized regime, the bed voidage is strongly dependent on both velocity and magnetic field strength. Porosity increases as the velocity increases but shows an exponential decrease as field intensity is increased,

4 - in the random motion regime, the voidage is strongly dependent on fluid velocity, increasing with it. However, it is little affected by magnetic field intensity.

Following the work by Kwauk et al. (1992) and Jovanovic et al. (1993), we propose here an equation to predict the average bed porosity for a given set of velocity and magnetic field intensity values:

$$\frac{H_{ms}}{1-\varepsilon} \ln\left(\frac{\varepsilon - \varepsilon_{ms}}{\varepsilon_{ff} - \varepsilon_{ms}}\right) = -(\alpha H^2 + \beta H) \qquad \text{(Eq. 6-7)}$$

or

$$\varepsilon = \varepsilon_{ms} + (\varepsilon_{ff} - \varepsilon_{ms}) \exp\left(-(1-\varepsilon)(\alpha H + \beta)\frac{H}{H_{ms}}\right) \qquad \text{(Eq. 6-8)}$$

These equations are valid for $U_0 \geq U_{mf}$ and $H < H_{ms}$ as long as magnetic saturation of the particles is not reached.

The term $\alpha H + \beta$ is the particles susceptibility as defined in Table 2-1. By multiplying it by H, we account for the particles magnetization intensity by volume. However, the particles do not occupy the entire volume of the bed. By multiplying the magnetization term by $1 - \varepsilon$, we account for the real volume that particles occupy in the bed.

In order to test the validity of Equation 6-8, we need to check the two limiting cases:

1 - at $H = 0$, for $U_0 > U_{mf}$, $\varepsilon = \varepsilon_{ff}$, which is satisfied by Equation 6-8,

2 - at $H = 0$ and $H_{ms} = 0$, we have $U_0 = U_{mf}$. We are at the minimum fluidization conditions where $\varepsilon_{ms} = \varepsilon_{ff} = \varepsilon_{mf}$. We need to obtain from Equation 6-8: $\varepsilon = \varepsilon_{mf}$. This condition is satisfied.

At $H = H_{ms}$, Equation 6-8 gives:

$$\varepsilon = \varepsilon_{ms} + (\varepsilon_{ff} - \varepsilon_{ms}) \exp\left(-(1-\varepsilon)(\alpha H_{ms} + \beta)\right) \qquad \text{(Eq. 6-9)}$$

For high fluidization velocities corresponding to high H_{ms} values, the exponential term in Equation 6-9 gets close to zero, and this equation may be used to estimate ε_{ms}.

Three parameters appear in Equations 6-7 and 6-8, ε_{ff}, ε_{ms} and H_{ms}. ε_{ff} is the porosity of the bed for a given velocity and $H = 0$. It can easily be calculated by the Richardson-Zaki equation (Eq. 2-2 and 2-3, Leva, 1959) as a function of the fluid velocity, the particles Reynolds number and their terminal velocity. H_{ms} was previously correlated to $\frac{U_0}{U_{mf}}$ (Eq. 6-2). However, we still need to correlate ε_{ms} to known variables and properties of the fluidizing system. An equation was found to predict the change in ε_{ms} as a function of $U_0 = U_{ms}$:

$$\frac{\varepsilon_{ms} - \varepsilon_{mf}}{\varepsilon_{mf}} = k\left(\frac{U_{ms} - U_{mf}}{U_{mf}}\right)^2 = k\left(\frac{U_0 - U_{mf}}{U_{mf}}\right)^2 \qquad \text{(Eq. 6-10)}$$

U_{mf} and ε_{mf} are characteristic of the particles and fluidizing fluid. Hence, in this equation, only one parameter, k, needs to be fitted. This was done by using the Least Squares Method as indicated in Appendix D. We obtain:

1 - for particles A:

$$\frac{\varepsilon_{ms} - \varepsilon_{mf}}{\varepsilon_{mf}} = 0.00382 \left(\frac{U_{ms} - U_{mf}}{U_{mf}} \right)^2 = 0.00382 \left(\frac{U_0 - U_{mf}}{U_{mf}} \right)^2$$

(Eq. 6-11)

2 - for particles B:

$$\frac{\varepsilon_{ms} - \varepsilon_{mf}}{\varepsilon_{mf}} = 0.0365 \left(\frac{U_{ms} - U_{mf}}{U_{mf}} \right)^2 = 0.0365 \left(\frac{U_0 - U_{mf}}{U_{mf}} \right)^2$$

(Eq. 6-12)

The predicted values given by Equations 6-11 and 6-12 and the experimental data are plotted against $\frac{U_0 - U_{mf}}{U_{mf}}$ in Figure 6-13.

As for parameters b and c appearing in Equation 6-2, we think it reasonable that k depends on the particles properties as well as on the vessel and distributor characteristics. The reason is the same as the one given at the end of Section 6.1 of this Chapter.

Now that we have defined ε_{ms}, we can go back to Equation 6-7. The predicted values given by this relationship and the experimental data are plotted against H in Figures 6-14 and 6-15 for particles A and B respectively. From these figures, we see that the way Equation 6-7 is stated allow all the data for different velocities to fall on a single curve. Velocity becomes an implicit variable of Equations 2-7 and 2-8, appearing in the expressions of ε_{ff}, ε_{ms} and H_{ms}.

Figure 6-13: Model fit for the prediction of ε_{ms}

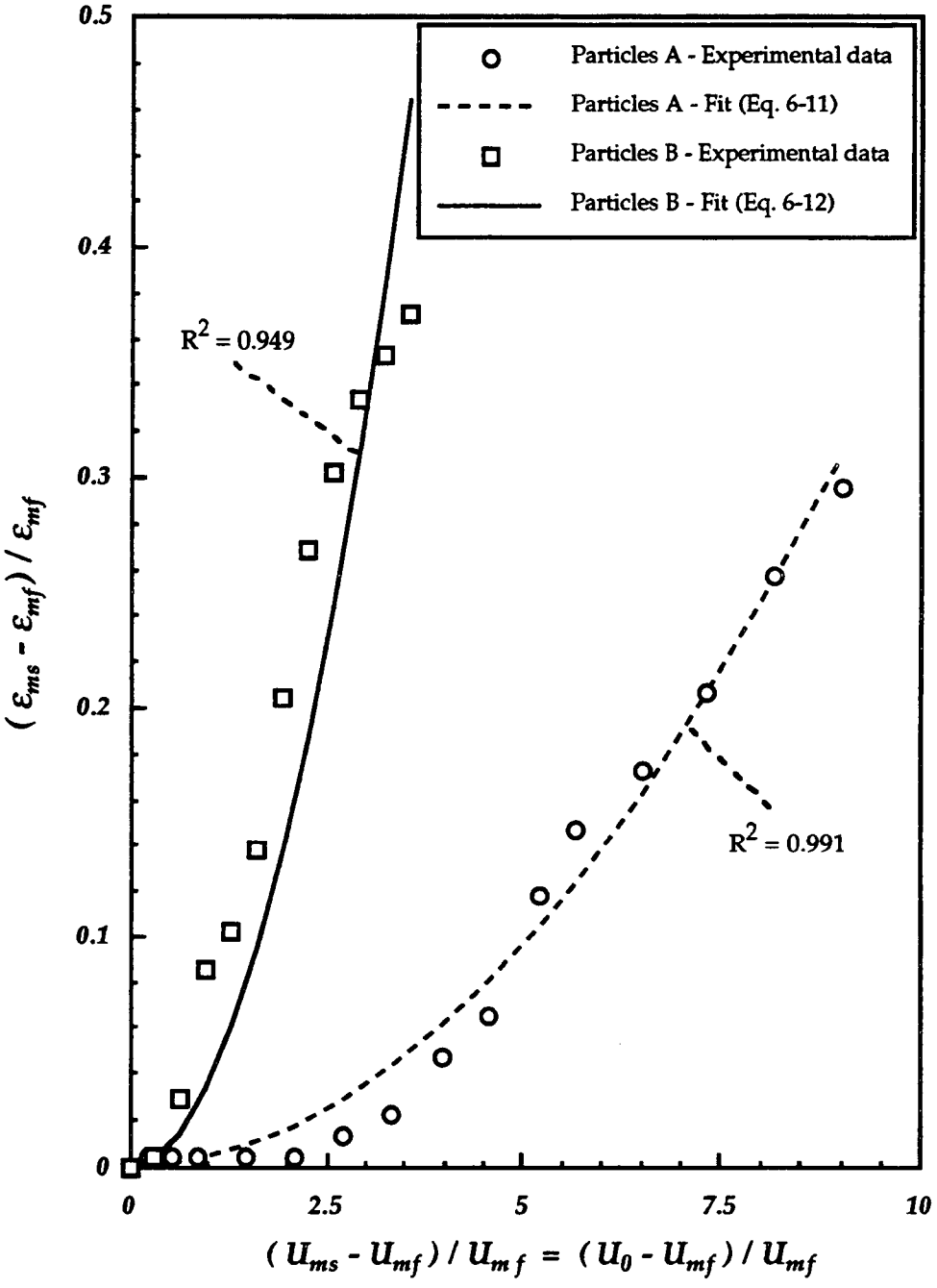

Figure 6-14: Model fit for the prediction of ε from Equation 6-7 for particles A

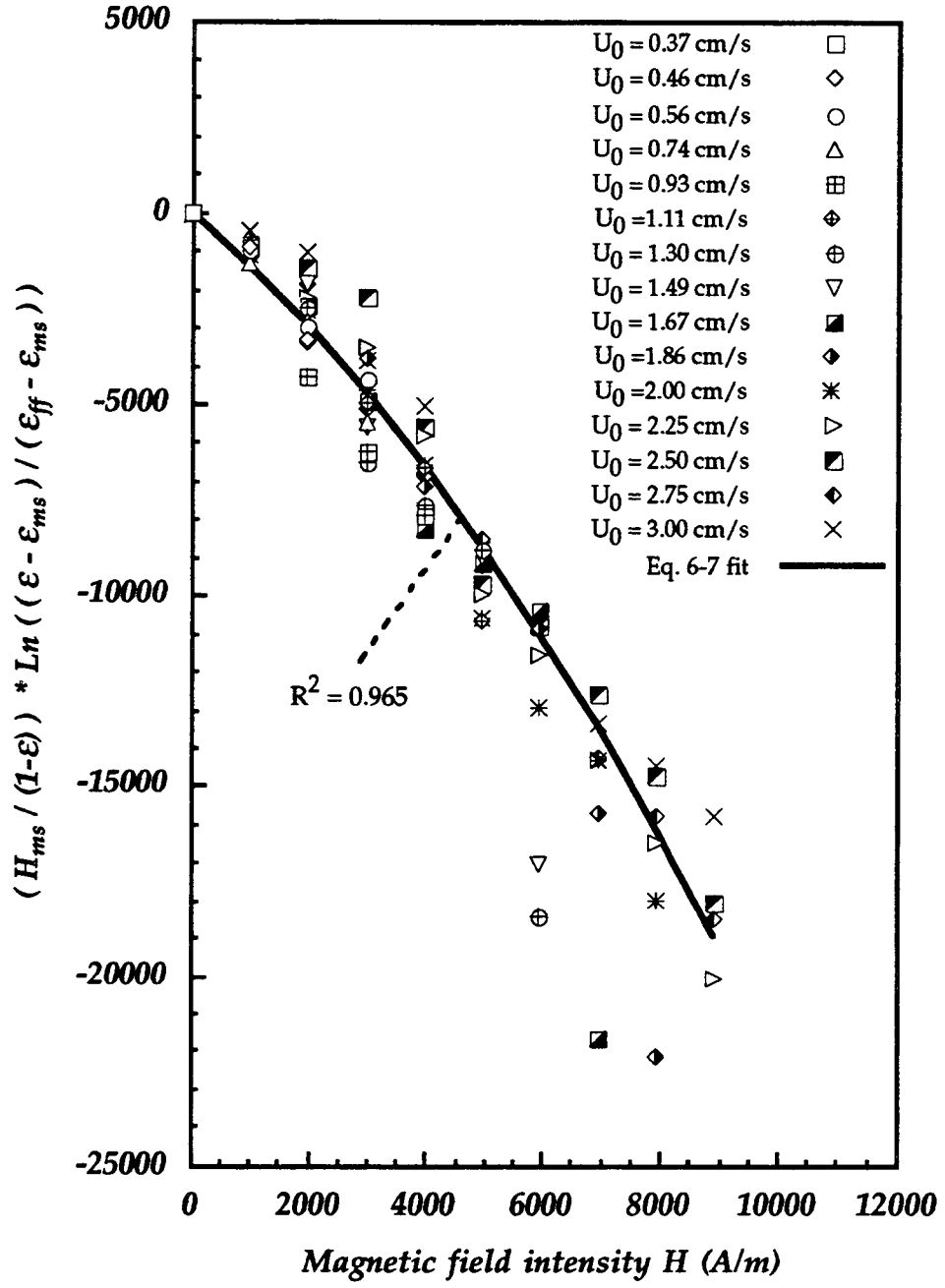

Figure 6-15: Model fit for the prediction of ε from Equation 6-7 for particles B

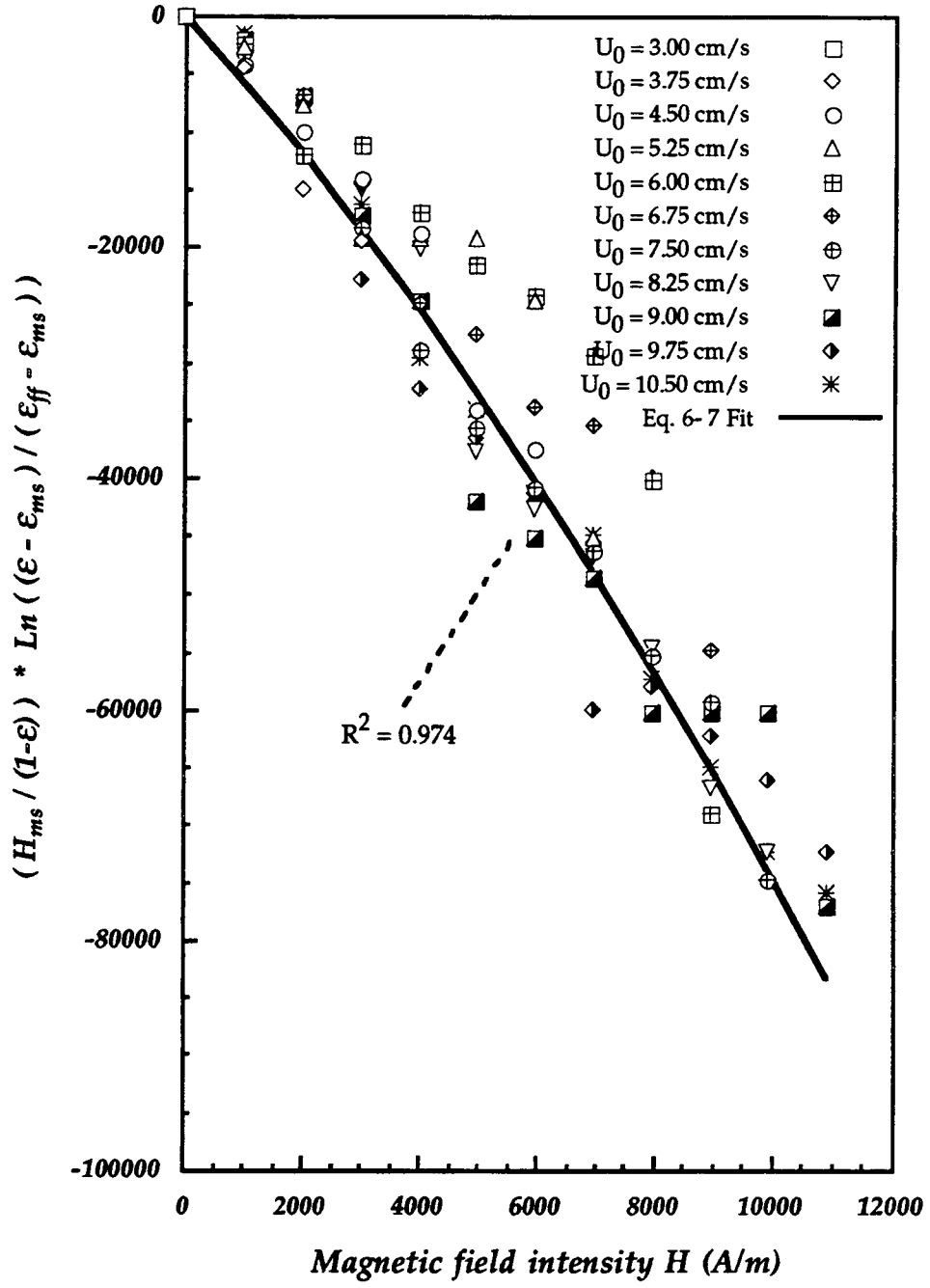

Introduction of magnetization intensity of the ferromagnetic particles is the key to the sucess of modeling the average bed porosity, and constitute an improvement to the correlations previoulsy published. The magnetization intensity of the particles allow our model to be applicable for different types of ferromagnetic particles.

CHAPTER 7
CONCLUSION AND RECOMMENDATIONS

This study was conducted to produce original experimental data and confirm that a magnetic field can substantially influence liquid fluidization of magnetic solids.

Three fluidizing regimes were observed for superficial velocities between the particle minimum fluidization velocity and terminal velocity. These results and observations are in general agreement with previous studies conducted by Kirko and Filippov (1960), Siegell (1987), Kwauk et al. (1992), Jovanovic et al. (1993):

1 - at low magnetic field intensities, particles behave discretely and move in random motion. In this random motion regime, voidage is little affected by the magnetic field. The pressure drop is constant and equal to the weight of particles per unit area of the bed,

2 - at higher magnetic field intensities, particles align themselves in chains parallel to the fluid flow and the magnetic field lines. In this partially stabilized regime, the bed becomes more structured as magnetic field strength is increased. The average bed porosity substantially decreases,

3 - at very high magnetic field intensities, particles become entirely immobile for all fluidization velocities. This is the stabilized regime. The bed porosity reaches a constant minimum value and is unaffected by further increase of the magnetic field strength. The pressure drop may increase depending on the additional net magnetic force and on the friction between the bed and the column walls.

Distribution of pressure drops along the bed height indicates that the bed porosity varies substantially from the bottom to the top of the bed. Typically, for high fluid velocities, three zones of different porosities can be detected. The zone next to the distributor has the smallest porosity value. This is also observed in ordinary fluidized beds (Kunii and Levenspiel, 1991). However, the applied magnetic field tends to make the bed more uniform in porosity.

The observed increase in the pressure drop across the bed in the partially stabilized and stabilized regimes in a uniform magnetic field is in contradiction with some of the previous studies (Filippov, 1960; Siegell, 1987). During fluidization, a point is eventually reached where the drag force exerted by the fluid on the agglomerated particles is not enough to support their weight. Particles "sink" toward the distributor and partially defluidize. They form, at the bottom of the column, a layer of magnetic material which attract particles from the upper part of the bed. This creates a net magnetic force on the fluidized particles toward the bottom of the bed. Particles are compacted at the bottom of the vessel. Eventually, the frictional forces between particles and the vessel walls become high enough not to be neglected when compared to the weight of particles per unit area. Hence, we can decomposed the pressure drop through the bed into three terms:

$$\Delta P_{bed} = \frac{W_f}{A} + \Delta P_m + \Delta P_f \qquad \text{(Eq. 6-6)}$$

where $\frac{W_f}{A}$ accounts for the weight of fluidized particles per unit area. ΔP_m is the additional pressure drop due to the magnetic net force acting on the particles attracted toward the bottom of the bed. ΔP_f accounts for the frictional force.

In this study an equation was found to predict the average bed porosity for given particles, velocity and magnetic field intensity:

$$\varepsilon = \varepsilon_{ms} + (\varepsilon_{ff} - \varepsilon_{ms}) \exp\left(-(1-\varepsilon)(\alpha H + \beta)\frac{H}{H_{ms}}\right) \qquad \text{(Eq. 6-8)}$$

with

$$\frac{U_0}{U_t} = \varepsilon_{ff}^{\,n} \quad \text{(Richardson-Zaki equation, Leva, 1959)} \qquad \text{(Eq. 2-2)}$$

$$\frac{\varepsilon_{ms} - \varepsilon_{mf}}{\varepsilon_{mf}} = k\left(\frac{U_{ms} - U_{mf}}{U_{mf}}\right)^2 = k\left(\frac{U_0 - U_{mf}}{U_{mf}}\right)^2 \qquad \text{(Eq. 6-10)}$$

and

$$\frac{U_0}{U_{mf}} = \frac{U_{ms}}{U_{mf}} = \frac{b}{M_{ms}}\left[e^{c H_{ms}} - 1\right] \qquad \text{(Eq. 6-2)}$$

where

$$M_{ms} = (\alpha H_{ms} + \beta) H_{ms} \qquad \text{(Eq. 6-3)}$$

In these equations, we see that magnetic properties of the particles, namely the magnetization intensity, play a major role in the behaviour of the MSFBs. Introduction of magnetization intensity in Equations 6-2 and 6-8 was the key to the success of modeling the average bed porosity. It allows the model to be applicable for different types of ferromagnetic particles and is an improvement to previous correlations. Coefficients b, c and k appearing in Equations 6-2 and 6-10 are believed to depend on particles, fluid and distributor plate characteristics.

For future study, we recommend extension of this work on particles with different magnetization susceptibilities so that proposed equations can be tested

more rigorously. This includes testing with composite particles as well as mixtures of ferromagnetic and nonmagnetic particles.

More work is needed to establish a relationship between the distributor plate characteristics and its influence on bed structure. One should determine the effect of distributor type (i.e. porous plate, perforated plate, ...), the effect of hole size in a perforated plate, the effect of hole location in a perforated plate.

Once above suggested studies are done, the mass and heat transfer in MSFBs has to be studied. The enhancement of mass and heat transfer rates in fluidized beds is what we are mainly interested in. The knowledge of how to design MSFBs and how to predict porosity, mass and heat transfer between fluid and particles will allow us to capitalize on the advantages of MSFBs over conventional fluidized beds.

BIBLIOGRAPHY

Arnaldos J., Casal J., Lucas A., and Puigjaner L., Magnetically stabilized fluidization: modeling and applications to mixtures, *Powder Technol., 44* (1985) 57

Bakker P. J. and Heertjes P. M., Porosity measurements in a fluidized bed, *Brit. Chem. Eng., 3* (1958) 240

Bakker P. J. and Heertjes P. M., Porosity distributions in a fluidized bed, *Chem. Eng. Sci., 12* (1960) 260

Bologa M. K. and Syutkin S. V., *Electron Obrab Mater, 68* (1977) 38

Burns M. A. and Graves D. J., Continuous affinity chromatography using a magnetically stabilized fluidized bed, *Biotechnol. Prog., Vol. 1, No. 2* (1985) 95

Chitester D. C. et al., *Chem. Eng. Sci., 39* (1984) 253

Davis G. F. and Levenspiel O., Theory and operational characteristics of the magnetic valve for solids, Part III: external coil design, *Powder Technol., 44* (1985), 19

Filippov M. V., The effect of a magnetic field on a ferromagnetic particle suspension bed, *Prik. Magnit. Lat. SSR, 12* (1960) 215

Filippov M. V., Resistance and expansion of a fluidized bed of magnetite in a magnetic field, *Latv. PSR Zinat. Akad. Vestis, 12* (No. 173) (1961) 47

Filippov M. V., Some properties of a suspended bed of ferromagnetic particles in a magnetic field, *Voprosy Magnitnoi Gidrodinamiki I Dinamiki Plazmy* (1962) 635

Filippov M. V., Fluidization of a suspended layer of magnetite in a magnetic field, *Latv. PSR Zinat. Akad. Vestis, 1* (No. 174) (1962) 69

Ivanov D. G. and Grozev G., *Mineral Torve Nauch Teck-Konf 2nd* (1970) 39

Jaraiz E., Wang Y., Zhang G. T., and Levenspiel O., Theory and Operational Characteristics of the Magnetic Valve for Solids, Part I: Grate Design, and Part II: Collar Design, *AICHE J., 30* (1984) 951 and 959

Jovanovic G. N., Sajc L., Jovanovic Z., Vunjak-Novakovic G., Pesic R., and Vukovic D., Magnetically controlled liquid-solid fluidized beds of ferromagnetic particles, 1993

Jovanovic G. N. and Jovanovic Z., A novel approach in controlling performance of fluidized beds: bubble size and fluidization regimes in magnetically controlled fluidized beds, AIChE 1993 Annual Meeting, November 7-12 1993, St. Louis, Missouri, Novel reactor techniques for heterogeneous systems symposium, Paper No. 28i (1993)

Kirko I. M. and Filippov M. V., Standard correlations for a fluidized bed of ferromagnetic particles in a magnetic field, Report F-21, Section on Physical Modeling, Interinstitutional Scientific Conference on Applied Physics and Mathematical Modeling, Moscow (1959); *Zh. Tek. Fiz., 30* (1960) 1081

Kunii D. and Levenspiel O., Fluidization Engineering, Wiley, New York (1991)

Kwauk M., Magnetic field controlled solids valve, *Inst. Chem. Metall., 1977 - 1 - 26*, 1977

Kwauk M., Ma X., Ouyang F., Wu Y., Weng D., and Cheng L., Magnetofluidized G/L/S systems, *Chem. Eng. Sci., 47* (1992) 3467

Leva M., Fluidization, McGraw Hill, New York (1959)

Liu Y. A., Hamby K., and Colberg R., Fundamental and practical developments of magnetofluidized beds: a review, *Powder Technol., 64* (1991) 3

Moiset P. and Dartois R., Magnetic regulation of underflow discharge of a dense media washing cone, *Proc. Intern. Min. Process. Cong.*, 1960, 565

Penchev I. P. and Hristov J. Y., Behaviour of fluidized beds of ferromagnetic particles in an axial magnetic field, *Powder Technol., 61* (1990) 103

Reitz J. R., Milford and Christy, Foundations of electromagnetic theory, Addison-Wesley Publishing Company (1992)

Rosensweig R. E., Fluidization: hydrodynamic stabilization with a magnetic field, *Science, Vol. 204 (6)* (1979 a) 57

Rosensweig R. E., Magnetic fluidization of the state of uniform fluidization, *Ind. Eng. Chem. Fundam., Vol. 18, No. 3* (1979 b) 260

Sada E., Katoh S., Shiozawa M. and Fukui T., Performance of fluidized bed reactors utilizing magnetic fields, *Biotechnol. Bioeng. 23* (1981) 2561

Shumkov S. H. and Ivanov D. G., Axial and radial density profiles in fluidized beds with and without electromagnetic fields, *Khim. Ind. 47 (No. 10)* (1975) 442

Shumkov S. H. and Ivanov D. G., Axial and radial density profiles in fluidized beds with and without electromagnetic fields, *Int. Chem. Eng., 17* (1977) 400

Siegell J. H., Liquid-fluidized magnetically stabilized beds, *Powder Technol., 52* (1987) 139

Siegell J. H., Magnetically frozen beds, *Powder Technol., 55* (1988) 127

Siegell J. H., Early studies of magneto-fluidized beds, *Powder Technol., 57* (1989) 213

Sonolikar R. L. et al, *Indian Journal of Technology, 10* (1972) 377

Sonolikar R. L., Magneto - fluidized beds, in L. K. Doraiswamy and A. S. Mujumbar (eds.), *Transport in fluidized particle systems* , Elsevier, Amsterdam, Netherlands (1989) 359

Terranova B. E. and Burns M. A., Continuous cell suspension processing using magnetically stabilized fluidized beds, *Biotechnol. Bioeng., 37* (1991) 110

Wallace A. K., Ranawake U. A. and Levien K., Experimental feasibility study of a magnetic elevator for particles, *Powder Technol., 64* (1991) 125

Y. Wang et al., A magnetic control valve for flowing solids (MVS): explanatory studies, *Ind. Eng. Chem., Process Des. Dev.* 21 (1982) 717

APPENDICES

APPENDIX A
PRESSURE DROP ACROSS THE DISTRIBUTOR PLATE

The pressure drop across the distributor is shown in Figure A-1. It is a quadratic function of water superficial velocity.

Figure A-1: Pressure drop across the distributor

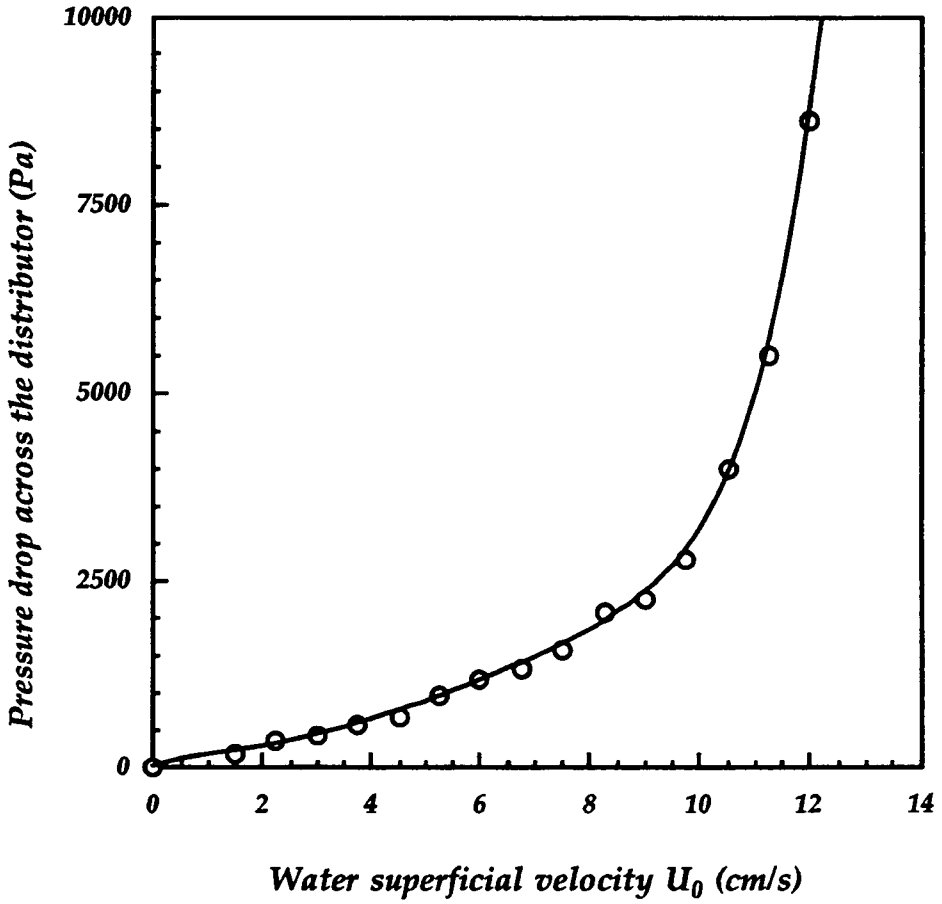

APPENDIX B
MAGNETIZATION CURVES FOR PARTICLES A AND B

The magnetization curves for particles A and B are shown in Figure B-1. They are used to determine the constant coefficient β in the expression of χ as a function of H:

$$\chi = \alpha H + \beta \qquad \text{(Eq. 2-6)}$$

χ is shown in Figure B-2 as a function of the magnetic field intensity for both types of particles.

Figure B-1: Magnetization curves for particles A and B

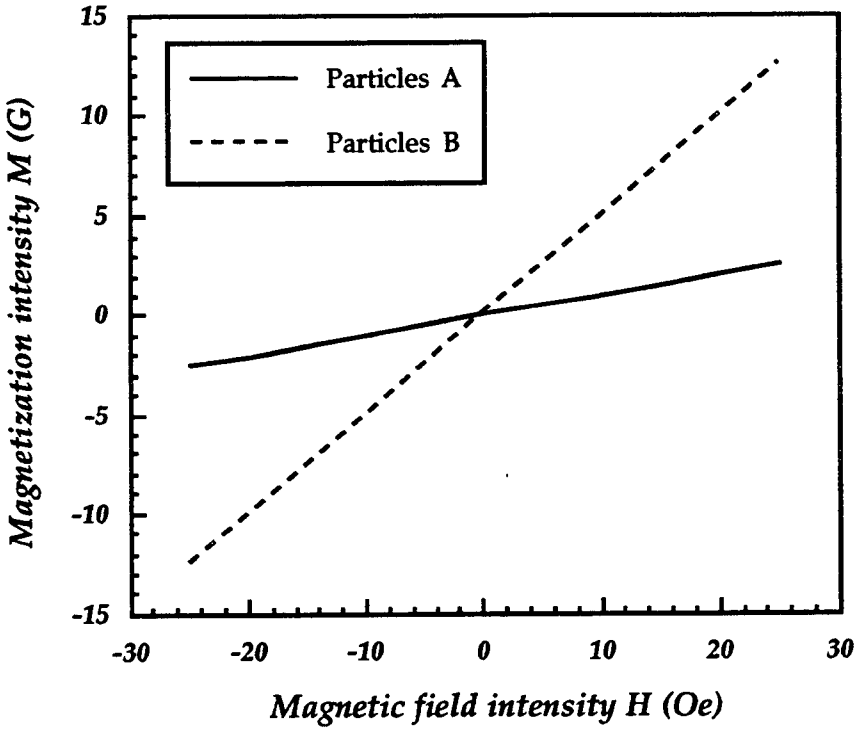

Figure B-2: Magnetic susceptibilities of particles A and B as a function of magnetic field intensity

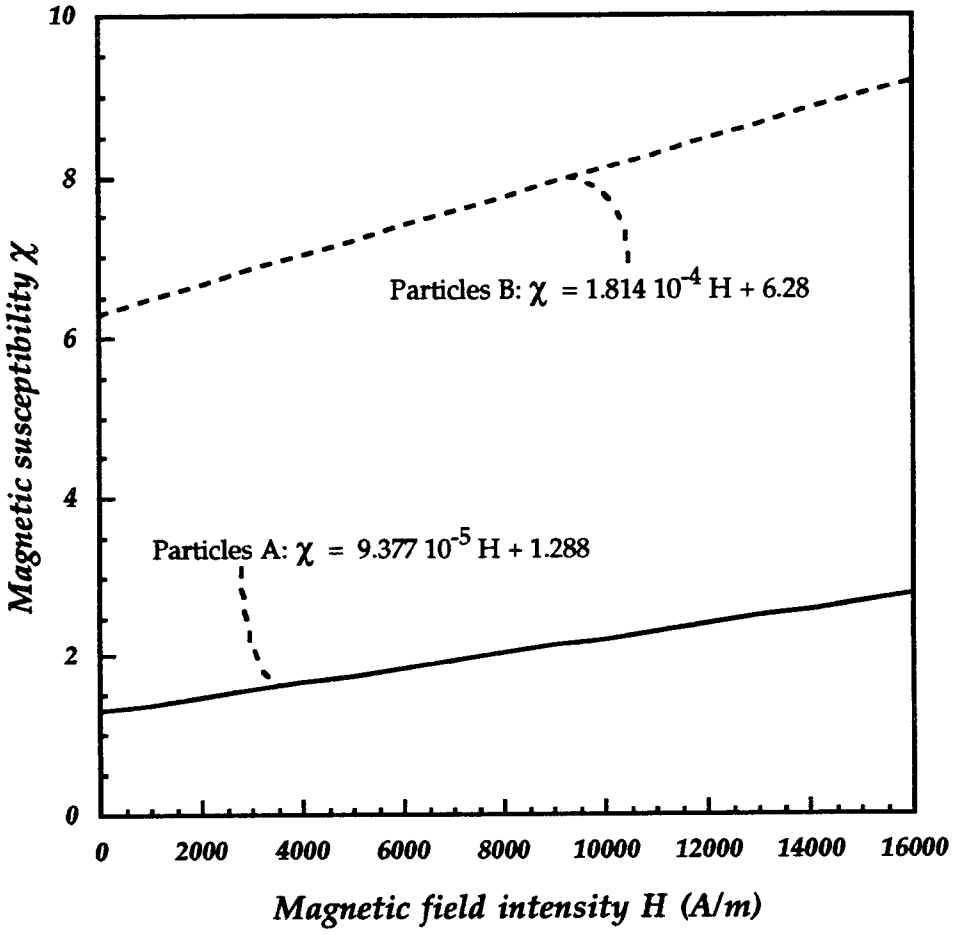

APPENDIX C
VOLTAGE - INTENSITY CALIBRATION CURVE FOR THE MAGNETIC FIELD GENERATOR

The voltage - intensity (U - I) calibration curve for the magnetic field generator (power supplies, copper coil, connecting wires) is displayed in Figure C-1. I is a linear function of U. The inverse of the slope gives the resistance of the whole electric circuit:

$$R = \frac{U}{I} \qquad \text{(Eq. C-1)}$$

Figure C-1: Voltage-current calibration curve for the magnetic field generator

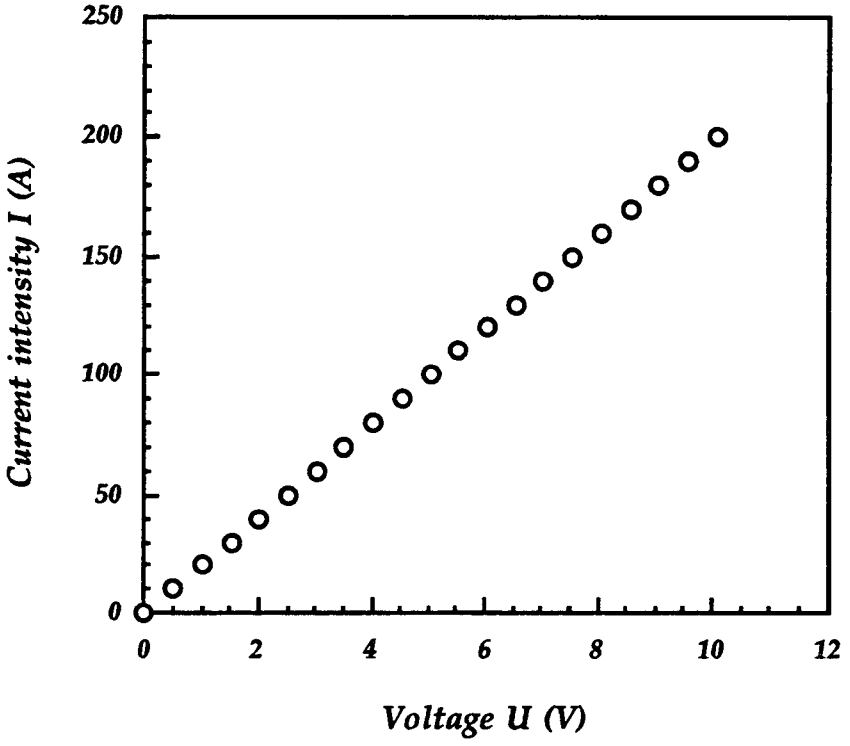

APPENDIX D
LEAST SQUARES METHOD FOR CURVE FITTING

This appendix is divided into two sections, each of which deals with the use of the Least Squares Method to fit a given type of function through data points:

1 - fit of an exponential function of the form $y = a_1 [\exp (a_2 x) - 1]$,

2 - fit of a quadratic function of the form $y = a_3 x^2$.

In the following sections we let x be the explanatory variable, Y be the experimental data points function of x and y be the predicted values.

To quantitatively determine the strength of the fit, we can compute:

$$R^2 = \frac{\sum_{j=1}^{J} Y^2 - \sum_{j=1}^{J} (Y - y)^2}{\sum_{j=1}^{J} Y^2} \quad 100\ \% \qquad \textbf{(Eq. D-1)}$$

D.1 - Fit of an exponential function $y = a_1 [\exp (a_2 x) - 1]$

This procedure was used to determine the parameters b and c appearing in Equation 6-1. They are equivalent to parameters a_1 and a_2 in Equation D-2:

$$y = a_1 [\exp (a_2 x) - 1] \qquad \textbf{(Eq. D-2)}$$

In order to find the best fit for Equation D-2 through experimental data points, we minimize the following sum of squares:

$$SS = \sum_{j=1}^{J} (Y - y)^2 \qquad \text{(Eq. D-3)}$$

$$= \sum_{j=1}^{J} (Y - a_1 [\exp(a_2 x) - 1])^2 \qquad \text{(Eq. D-4)}$$

In order to find a_1 and a_2 such that the sum is minimized, we need to have:

$$\frac{d\,SS}{d\,a_1} = 0 \qquad \text{(Eq. D-5)}$$

and

$$\frac{d\,SS}{d\,a_2} = 0 \qquad \text{(Eq. D-6)}$$

Equations D-4 and D-5 lead to:

$$a_1 = \frac{\sum_{j=1}^{J} Y - \sum_{j=1}^{J} Y \exp(a_2 x)}{\sum_{j=1}^{J} \exp(2a_2 x) - 2 \sum_{j=1}^{J} \exp(a_2 x) + 1} \qquad \text{(Eq. D-7)}$$

From Equations D-4 and D-6 we have:

$$a_1 \sum_{j=1}^{J} x \exp(2a_2 x) - \sum_{j=1}^{J} Y x \exp(a_2 x) - a_1 \sum_{j=1}^{J} x \exp(a_2 x) = 0 \qquad \text{(Eq. D-8)}$$

a_1 and a_2 can be found by solving simultaneously Equations D-7 and D-8.

D.2 - Fit of a quadratic function $y = a_3 x^2$

This procedure was used to determine the parameter k appearing in Equation 6-8. k is equivalent to the parameter a_3 in Equation D-9:

$$y = a_3 x^2 \qquad \text{(Eq. D-9)}$$

In order to find the best fit for Equation D-9 through experimental data points, we minimize Equation D-3, which can be expressed as:

$$SS = \sum_{j=1}^{J} (Y - a_3 x^2)^2 \qquad \text{(Eq. D-10)}$$

In order to find a_3 such that the sum of squares is minimized, we need to have:

$$\frac{d\,SS}{d\,a_3} = \sum_{j=1}^{J} (-2 x^2 Y + 2 a_3 x^4) = 0 \qquad \text{(Eq. D-11)}$$

or

$$a_3 = \frac{\sum_{j=1}^{J} Y x^2}{\sum_{j=1}^{J} x^4} \qquad \text{(Eq. D-12)}$$